PUBLICATIONS OF THE ASTRONOMICAL SOCIETY OF THE PACIFIC, **110**:533–552, 1998 May

Homogeneous Photometry for Star Clusters and Resolved Galaxies. I. A Survey of Bright Stars in the Fornax Dwarf Spheroidal Galaxy

PETER B. STETSON[1,2] AND JAMES E. HESSER[1]

National Research Council, Herzberg Institute of Astrophysics, Dominion Astrophysical Observatory, 5071 West Saanich Road, Victoria, British Columbia, V8X 4M6, Canada; Peter.Stetson@hia.nrc.ca, James.Hesser@hia.nrc.ca

AND

TAMMY A. SMECKER-HANE

Department of Physics and Astronomy, 4129 Physical Sciences 2, University of California, Irvine, CA 92697-4575; smecker@carina.ps.uci.edu

Received 1997 December 3; accepted 1998 January 27

ABSTRACT. We present accurate photometry on the Johnson *B*, Kron-Cousins *R* photometric system for approximately 100,000 stars in a $\frac{1}{3}$ deg^2 field centered on the dwarf spheroidal galaxy in Fornax. We identify numerous probable short-period variable stars, blue stars that appear to be the main sequence of a small population with an age of order 10^8 yr, and two distinct types of luminous red star: an extended sequence of primarily carbon stars and a clump of mostly M giants slightly more luminous than the giant-branch tip. The spatial distribution of each of these subpopulations within the Fornax dwarf galaxy is considered.

1. INTRODUCTION

Dwarf galaxies are the simplest galaxies and thus the best places to study the processes that regulate star formation and galaxy evolution. However, many questions about the evolution of dwarf galaxies remain to be answered. What are their star formation histories? How has their gas content evolved with time? What are the important physical mechanisms that shape their evolution and create the observed scaling laws between mass, luminosity, and metallicity? We have a unique opportunity to investigate these issues by studying the dwarf galaxies in the Local Group. Their proximity allows us to make detailed measurements, *on a star-by-star basis*, of the ages and chemical abundances of their stellar populations and thus read the fossil record of the evolution of these galaxies.

The dominant type of dwarf galaxy in the Local Group by number is the dwarf spheroidal galaxies (dSphs). These systems are characterized by their low luminosities ($-9 \lesssim M_V \lesssim -14$), small spatial extent (core radii $\lesssim$ a few hundred parsecs), low stellar density (central surface densities $\Sigma_V \lesssim 0.002\ L_\odot\ \mathrm{pc}^{-2}$), lack of neutral hydrogen (upper limits to the mass in H I are less than $10^4\ M_\odot$), lack of current star formation (e.g., no H II regions are seen), and the presence of dark matter (typical mass-to-light ratios are of order several tens). Soon after the discovery of the first dwarf spheroidals by Shapley (1938), it became commonplace to regard them as the least luminous ellipticals, or—equivalently, as was then thought—the loosest globular clusters, and thus paradigms of pure Population II (see, e.g., Baade 1944). However, correlations among certain fundamental properties (luminosity, surface brightness, effective radius, central velocity dispersion) discovered by Kormendy (1985) suggested that the dSphs should be regarded not as "the littlest ellipticals," but rather as "the gas-poorest irregulars." In confirmation, new color-magnitude diagrams (CMDs) and spectroscopy of individual red giants in several of the systems have shown us that, in spite of their current quiescent appearance, most of the dSphs have had surprisingly complicated evolutionary histories. (For recent reviews, see Smecker-Hane 1997 and Da Costa 1997a, 1997b.)

To summarize what is currently known, the Ursa Minor dSph is the only one thought to contain *only* old, metal-poor stars similar to those found in Galactic globular clusters (Olszewski & Aaronson 1985). Sculptor and Draco, too, are both predominantly old (Da Costa 1984; Stetson, McClure, & VandenBerg 1985; Carney & Seitzer 1986; Grillmair et al. 1997), but each of them either experienced a trickle of continuing star formation or has an unusually extensive population of blue stragglers (Da Costa 1984; Stetson 1997). There is spectroscopic evidence for a range of metal abundance within both Ursa Minor and Draco (Zinn 1978, 1981; Kinman, Kraft, & Suntzeff 1981; Stetson 1984; Suntzeff et al. 1984; Lehnert et al. 1992), although these conclusions are based on relatively poor-quality

[1] Visiting Astronomer, Cerro Tololo Inter-American Observatory, which is operated by the Association of Universities for Research in Astronomy, Inc., under contract with the National Science Foundation.

[2] Guest User, Canadian Astronomy Data Centre, which is operated by the Dominion Astrophysical Observatory for the Canadian National Research Council's Herzberg Institute of Astrophysics.

data compared to what can now be obtained for globular cluster giants. Consequently, if these systems are self-enriched, they must have created multiple generations of stars within whatever star formation epoch was available to them. The Sextans dSph, while containing a predominantly metal-poor, old population, also exhibits a small but, in this case, well-determined internal dispersion in metallicity [σ([Fe/H]) $\approx$ 0.2 dex; Suntzeff et al. 1993].

The other dSphs that have been imaged with modern (i.e., large-format, low-noise, high quantum efficiency) detectors all show more complex histories. The bulk of stars in the Leo I dSph are only ~3 Gyr old (Lee et al. 1993; Mateo et al. 1994), while those in the Leo II dSph are 7–14 Gyr old (Mighell & Rich 1996). The ages of stars in the Carina dSph span ~2–14 Gyr and show a surprisingly long gap in the star formation history that lasted from 8 to 12 Gyr ago (Mighell 1990; Mighell & Butcher 1992; Smecker-Hane et al. 1996). Although numerous generations of stars formed in the Leo II and Carina dSphs, their red giant branches are narrow, suggesting that their internal dispersions in metallicity are no larger than in Sextans, σ([Fe/H]) $\lesssim$ 0.25 dex. To produce such small ranges in metallicity while exhausting the galactic reservoir of gas, newly synthesized metals must have been lost in supernova-driven galactic winds or stripped by collisions with Galactic halo gas. The former explanation is generally preferred because the dSphs do follow global scaling relations, and thus the mechanisms that govern their evolution should be predominantly internal rather than external. Consistent with their larger masses, the Fornax and Sagittarius dSphs show even more range in age and metallicity. Both have internal metallicity dispersions of at least 1.0 dex (Buonanno et al. 1985; Beauchamp et al. 1995; Sarajedini & Layden 1995). Initial estimates of the star formation history of the Sagittarius dSph suggest a large range in age with possible peaks at ~4 and 10 Gyr ago (Mateo et al. 1995; Fahlman et al. 1996). The star formation rate in the Fornax dSph may have been roughly continuous until about 2 Gyr ago, when it decreased substantially (Smecker-Hane 1997). However, as discussed in this paper, a small population of stars possibly as young as 10^8 yr are seen in the Fornax CMD.

The fact that we find evidence of star formation epochs that spanned a good fraction of the Hubble time teaches us an important lesson: star formation must be self-regulated even in these very low-mass galaxies. Once we measure the exact star formation and chemical evolution histories of the dSphs, we can determine the physical mechanisms that regulated their evolution, be they photoionization from massive stars or the metagalactic UV background, energetic input from stellar winds or supernova explosions, and/or massive dark matter halos. Another important lesson is that gas may remain inside dSphs for many gigayears. The very young stars we see in the Fornax system suggest that sensitive searches for gas in neutral and ionized form might reveal the physics that makes the gas stable against star formation for long periods of time. However, the great variety of star formation histories among the few examples available to us should also serve as a warning that many different mechanisms may be of comparable importance, and the way they play against each other may be very sensitive to individual circumstances.

We have undertaken a series of studies to determine the star formation and chemical evolution histories of several of the Local Group dSph galaxies using CMDs and spectroscopy of individual red giant stars. In this paper, we present photometry for approximately 10^5 of the brightest stars in the central $\frac{1}{3}$ deg^2 region of the Fornax dSph. These data were obtained to identify for future spectroscopic analysis a large sample of luminous red and blue members spanning a major fraction of the face of the galaxy, but it happens that these data are also capable of yielding information on the present-day spatial distribution of various stellar populations within Fornax. This forms the subject of the present paper. In a future paper, these data will be combined with deeper photometry of a smaller field, and a full analysis of the resulting CMD and its implications for the star formation history of Fornax will be undertaken. Eventually, the photometric results will be combined with spectroscopic data, which will allow comprehensive modeling of the chemical and kinematic evolution of Fornax.

2. OBSERVATIONS AND REDUCTIONS

Observations for this program were obtained on the four nights 1995 December 14/15–17/18, with the Tek2k_4 CCD at the f/7.5 Ritchey-Chrétien focus of the Cerro Tololo 1.5 m telescope. Tek2k_4 has 24 μm pixels, yielding an effective scale of 0.″435 pixel^{-1} and a full field 14.′8 square. The data were analyzed using the DAOPHOT/ALLFRAME suite of computer programs (Stetson 1987, 1994) and other domestic software (see, e.g., Stetson 1993).

Fornax was the first object observed each night. Pairs of frames were obtained in the standard *B* and *R* filters for each of nine subfields in the galaxy: one near the center of the galaxy and roughly coinciding with the 1994 Cerro Tololo 4 m prime-focus images of Smecker-Hane et al. (1998); four fields offset from the central field by roughly 10′ to the northeast, southeast, southwest, and northwest; and four more offset from the central field by roughly 14′ north, east, south, and west. Figure 1 is a montage of all of our *R*-band images of Fornax, illustrating the total field covered. By counting the nonempty pixels in this montage and in a similar one for the *B* images, we calculate that the area contained within at least one *B* image *and* at least one *R* image is 1274 arcmin^2; this total excludes parts of the field obliterated by the saturated images of very bright stars or by charge overflow from such stars.

On any given night, the nine subfields were observed in an erratic order, in the hopes of minimizing the aliasing of RR Lyrae variables. A total of 44 frame pairs were obtained for Fornax in the four nights. Exposure times were 600 s in *R* and 900 s in *B*, except for the central field, where exposures of 200

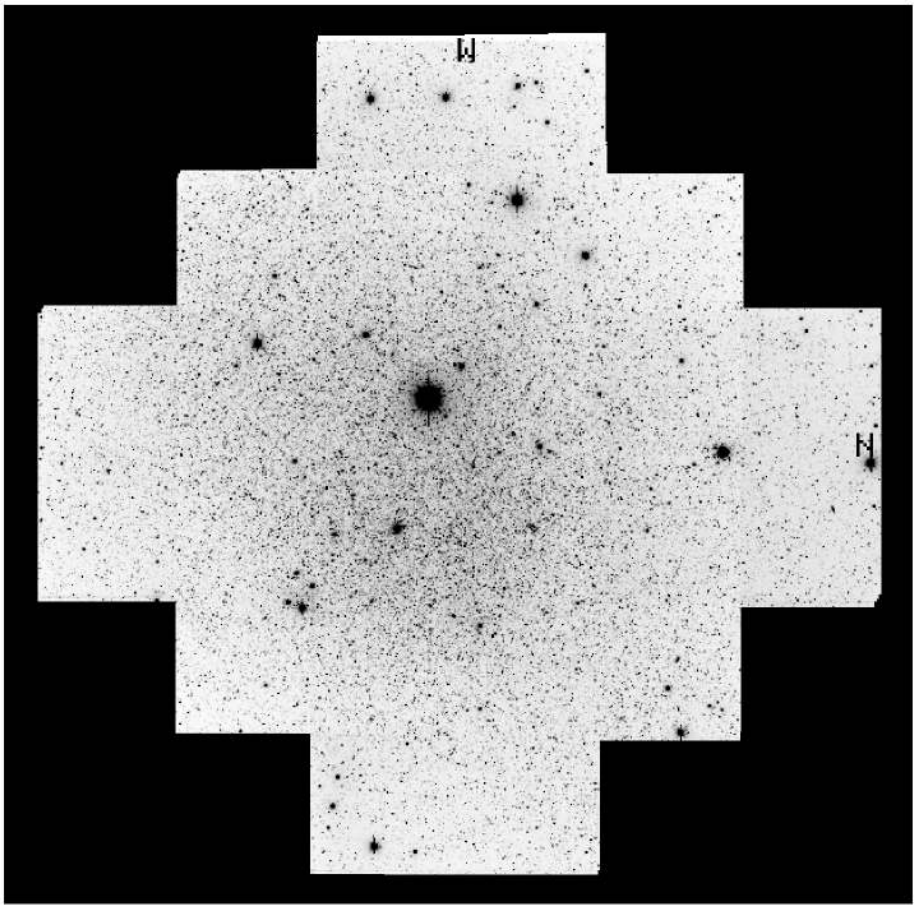

FIG. 1.—Digital montage of 44 *R*-band images of the Fornax dwarf spheroidal galaxy. North is to the right and west is up. Individual frames are 14′.8 on a side, and the montage as a whole is 43′.2 long and high.

and 300 s were obtained instead. The purpose of these shorter exposures was to minimize the saturation of bright stars in the central field so that, in conjunction with the 4 m observations, our data would span the widest possible range of magnitude for at least the central field of Fornax. The central field was also completely covered by overlap from the northeast, southeast, southwest, and northwest fields, so that despite the shorter exposure times for the central pointings, the magnitude limit is not any shallower in this part of the galaxy than in any other. Figure 2 illustrates as a gray-scale map the total number of exposures available for each part of the Fornax field: a small rectangular region in the center of the galaxy, roughly 30″ on a side, was contained in 24 frame pairs. The extremities of the off-center fields were in general contained within five frame pairs, except for the outboard corner of the southeast field and the outer end of the west field, which were contained within only four frame pairs each. Of course, around the very fringes of the area covered, small pointing offsets produced narrow zones where there are even fewer than four frame pairs available. Vertical narrow black streaks in Figure 2 represent columns where the data were obliterated by charge overflow from bright stars.

Only the third night of our run was completely photometric from beginning to end. The second night began with thin clouds, but it cleared off as we were obtaining our sixth exposure and was photometric thereafter. The availability of both photometric and nonphotometric data affects the course of the subsequent reductions. CCD photometry can be analyzed in either of two modes: absolute photometry, which for a number of decades was done mostly with photomultipliers, requires photometric conditions and involves solving for atmospheric extinction and absolute photometric zero points for the telescope/filter/detector system; the second mode, mimicking photographic photometry, is strictly differential in the sense that it does not require photometric conditions and does not attempt to measure the extinction or establish fundamental system zero points but does require a network of local photometric standards in every field studied. The color terms in the transformation from observed to standard-system magnitudes can be defined in either reduction mode, provided only that standard stars

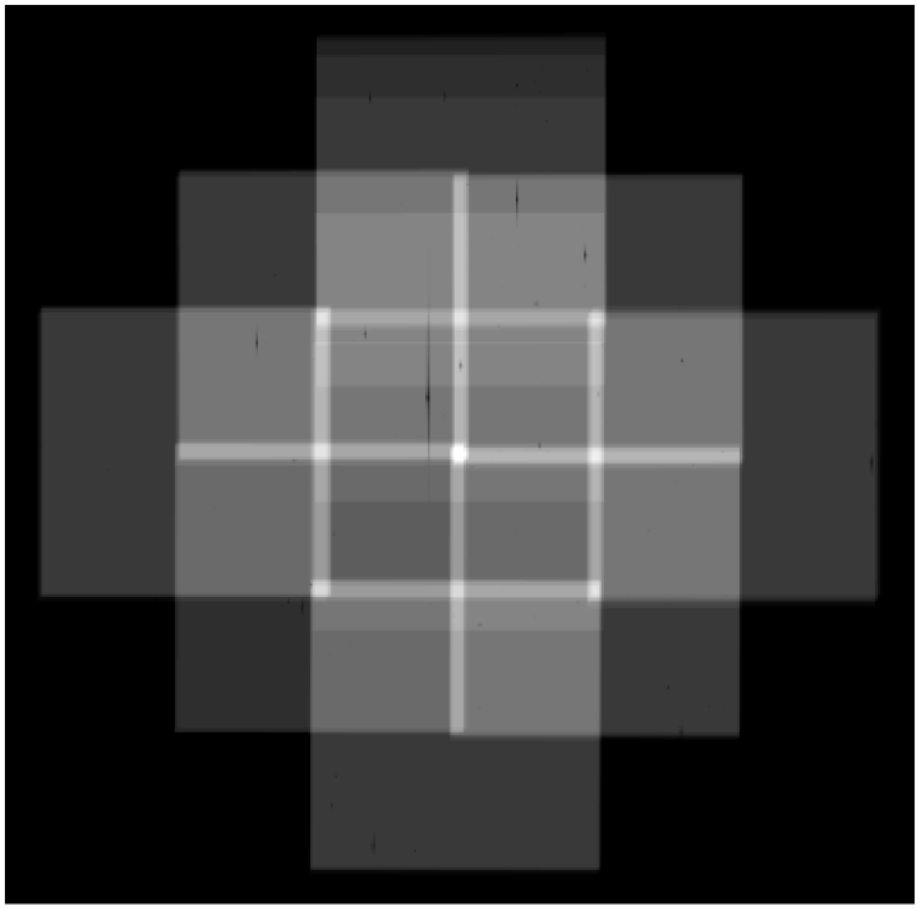

FIG. 2.—Map of total exposure time as a function of position within the field. Lighter-colored areas appeared in more frame pairs, ranging from the small bright square at the center representing a small region that was recorded in 24 frame pairs, to the dark quadrant in the southeast (*bottom left*) and the rectangle at the end of the west region (*top*) that appeared in four frame pairs each. Black regions in the interior of the map represent locations where saturated stars and charge overflow therefrom eradicated the photometric data.

spanning a significant range of intrinsic color be available in at least some of the fields observed if conditions are nonphotometric. Accordingly, we reduced all our data from night 3 and all but the first three frame pairs of night 2 in the "photomultiplier" mode and reduced the remainder of the data in "photographic" mode.

During the course of each of nights 1, 2, and 3, observations were also made of several Landolt (1973, 1992) equatorial and/or Graham (1982) E-region standard fields, as well as of several open and globular clusters, which Stetson (1998) is establishing as secondary standard fields. Fornax began each night near the zenith, and we observed it continuously until it reached an air mass of approximately 2.0 in the west. The generous overlap among our subfields provided an abundance of repeatedly observed stars that, in combination with our observations of Landolt and Graham fields at a variety of air masses, provided quite solid determinations of the extinction in B and R for the photometric nights. Quadratic color transformations were determined from the standard-field data independently for each of the first three nights. The second-order coefficients were small (<0.005 mag mag^{-2}), but not statistically insignificant in the case of the R filter; a mean of the three determinations of the second-order coefficient for each filter was calculated and was then imposed on the photometric transformations for each of the four nights. The Fornax observations that were obtained under photometric conditions enabled us to define 1060 local standards that met the following conditions: each was observed at least eight times under photometric conditions in both filters; each had a standard error of the mean magnitude less than 0.02 mag in both filters; none showed evidence of intrinsic variation—epoch-to-epoch magnitude differences greater than those expected from read noise and photon noise—in excess of 0.05 mag (the median value of this quantity was 0.009 mag). This local standard sequence enabled us to place the photometric and nonphotometric observations of Fornax on the same magnitude system to ± 0.001 mag (typical uncertainty in the relative zero point of one frame relative to the average of all frames).

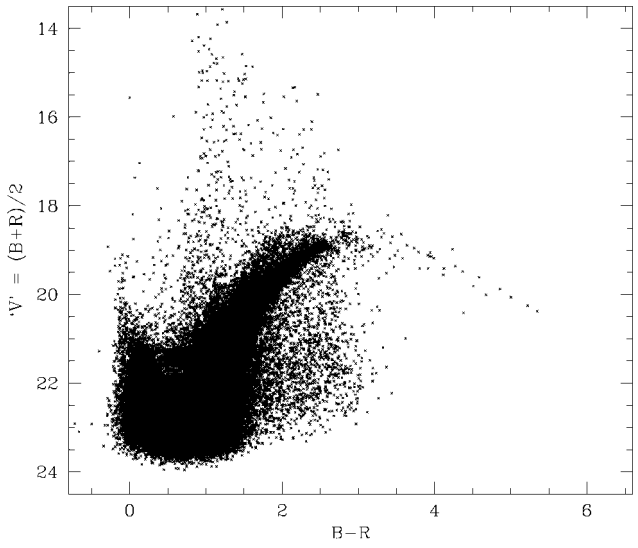

FIG. 3.—"*V*" vs. $B - R$ CMD for 91,911 stars in the Fornax survey area with $\sigma(B - R) < 0.1$ mag.

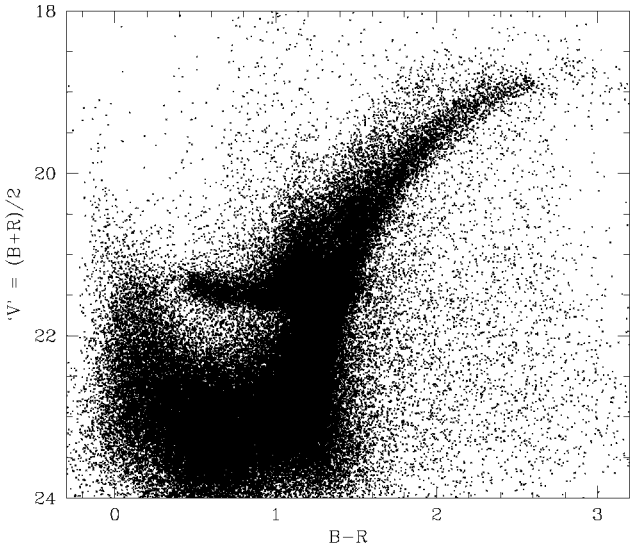

FIG. 4.—Expanded CMD for the Fornax galaxy. No selection on the basis of $\sigma(B - R)$ has been imposed.

3. DISCUSSION

3.1. Color-Magnitude Diagram

We obtained photometric measurements for a total of 115,840 detected objects in the Fornax field; of these, 115,052 had at least one valid measurement in each filter. From our calibrated photometry of these stars, we derived the magnitude "*V*" $\equiv (B + R)/2$ and the color $B - R$. A CMD for 91,911 stars with $\sigma(B - R) < 0.10$ mag on this photometric system[3] is presented in Figure 3. The member stars of Fornax itself fill the bottom left quadrant of the image, with a populous, broad giant branch pointing toward the center of the plot. There is a noteworthy sequence of several dozen very red, luminous stars extending from the tip of the giant branch down and toward the red, reaching nearly to ($B - R$, "*V*") = (5.5, 20.5); presumably these define the luminous tip of the double-shell-source stars in a young or intermediate-age stellar population, and many of them are likely to be carbon stars. A curious clump of a few dozen stars floats just to the red and above the well-defined tip of the red giant branch, at ($B - R$, "*V*") ~ (2.8, 18.7); this appears to be separated by a small gap from the principal giant branch, and its relationship to the long, narrow sequence of carbon stars is unclear. A range of sparsely populated giant branch tips fans blueward from the principal giant branch, with the bluest sequence perhaps terminating near ($B - R$, "*V*") ~ (1.9, 18.5). The main sequence of a very young stellar population can be perceived bluer than $B - R = 0.0$, and extending up to "*V*" ~ 19. A stubby-shaped horizontal branch can just be seen extending from the giant branch leftward across the Hertzsprung gap at "*V*" ~ 21.4. Stars brighter than "*V*" = 18.5 appear to be primarily of the foreground thick disk, with its main-sequence turnoff defining the vertical edge near $B - R \sim 0.8$; the half-dozen bright stars bluer than this limit may be thick-disk blue stragglers, or perhaps the high-*z* fringe of the thin disk. The population of thick-disk main-sequence stars continues faintward across the distribution of evolved Fornax stars, and the K and M dwarfs of the thick disk are presumably responsible for nearly all of the cloud of stars between Fornax's giant branch and $B - R \sim 3.5$.

Figure 4 is an enlargement of the lower left quadrant of Figure 3, except that in this figure no limit has been placed on $\sigma(B - R)$. The symbol size has been reduced to reveal more of the structure in the horizontal branch. Demers, Irwin, & Kunkel (1994) identified a population of blue stars in Fornax, with colors $B - V \sim 0$, and assumed that they are blue horizontal-branch stars. This identification is unlikely, since in our CMD the blue stars form a vertical sequence that, both above and below the horizontal branch, is rather cleanly separated from the red stars, while the horizontal branch itself (at "*V*" ~ 21.4) does not appear to extend as blue as $B - R = 0$. The red clump of youngish core helium-burning stars is still saturated

[3] We prefer to work with the pseudo-visual magnitude "*V*" rather than constructing a ($B - R$, *B*) or ($B - R$, *R*) CMD for a number of minor reasons. First, it lends a slightly more familiar appearance to the CMD. Second, the error in the "visual" magnitude is $\frac{1}{2}\,[\sigma^2(B) + \sigma^2(R)]^{1/2}$, which tends, in general, to be smaller than either $\sigma(B)$ or $\sigma(R)$. Third, the typical error in the "*V*" magnitude is more nearly orthogonal to the error in the color, whereas if *B* or *R* were to be plotted against $B - R$, photometric errors would produce tilted error ellipses in the CMD. For both of these latter two reasons, when we isolate small regions of the CMD for consideration later in this paper, the use of "*V*" as the magnitude in preference to *B* or *R* will render magnitude errors more nearly negligible in comparison to color errors and will reduce sample bias due to edge effects at the boundaries of the selected regions.

even in this expanded plot, so the horizontal-branch region of the CMD is enlarged yet again in Figure 5. Here we can see that the red clump has a dominant, nearly circular, component with a bit of a comet-like tail extending redward and overlapping the giant branch, and a thin halo on the brightward but not the faintward side. The extended horizontal branch presumably belonging to the oldest and most metal-poor populations in Fornax is 0.1 or 0.2 mag fainter than the dominant clump, as also seen in Carina (Smecker-Hane et al. 1994), and extends blueward across the center of the diagram to a color $B - R \sim 0.8$, where there may be a bit of a gap separating it from the tilted bar of RR Lyraes (which are bluer when they are bright and redder when they are faint; see, e.g., Smith 1995, Fig. 1.9). Again, there does not appear to be a strong component of the horizontal-branch population extending even as blue as $B - R = 0.3$; instead, the horizontal branch probably terminates inside the instability strip.

If we take the horizontal branch seen at "V" $\sim$ 21.4 to have an absolute magnitude in the range $0.6 \lesssim M_V \lesssim 1.0$, and if the brightest blue stars represent a main sequence terminating at "V" $\sim$ 19.2, then this corresponds to a turnoff luminosity of $M_V \sim -1.4$ and $M_{\rm bol} \sim -3$, and an age in the neighborhood of 10^8 yr regardless of the assumed metal abundance (see, e.g., Bertelli et al. 1994; cf. their Fig. 7). If the few blue stars with "V" < 19.2 are also taken to be on the main sequence, the age could be a bit younger, while if it were the case that the brightest few blue stars are all binaries, blends, highly evolved stars, or some type of rare foreground star, the minimum age could be somewhat greater. For instance, if the true turnoff were actually at "V" $= 20.2$, the implied age could be as great as 2×10^8 yr.

3.2. Red Stars

Luminous carbon stars, such as those in dwarf spheroidal galaxies, are commonly recognized as representatives of an intermediate-age component (see, e.g., Da Costa 1997b and references therein). These stars may be divided into two categories: the "normal" carbon stars that appear to be evolved double-shell-source giants whose surface layers are enriched in carbon by convective dredge-up during thermal pulses in the helium-burning shell; and a class of fainter, bluer carbon stars identified in the galactic bulge whose physical nature is not yet well understood (Westerlund et al. 1991; see also Azzopardi & Lequeux 1992). (A third type, the dwarf carbon star—see, e.g., Dearborn et al. 1986; Green, Margon, & MacConnell 1991—is not at present accessible to observation in the dwarf spheroidal galaxies.) Of these two, the former type is of the most immediate interest, because normal carbon stars can often be recognized by their very red broadband colors.

Demers & Kunkel (1979, hereafter DK) blinked a *B*, *V* pair of plates obtained with the CTIO 1.5 m telescope and identified 66 very red stars in the field of Fornax. Aaronson & Mould (1980) subsequently used the CTIO 4 m telescope to obtain

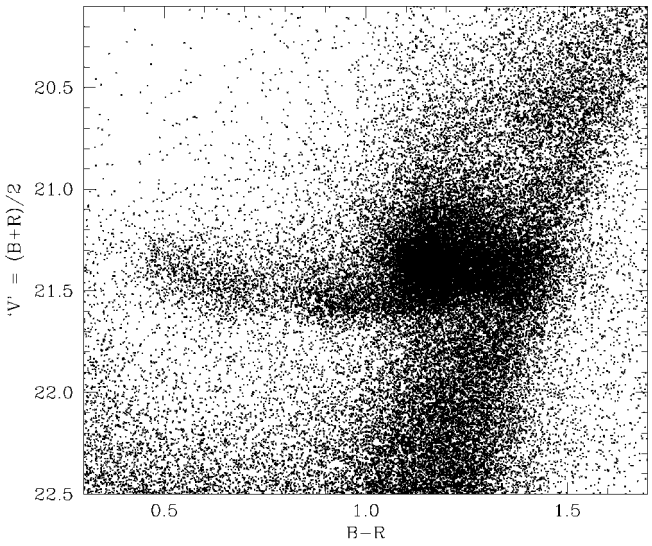

FIG. 5.—Expanded view of the CMD of the Fornax galaxy, revealing structure in the distribution of core helium-burning stars.

Vidicon spectrophotometry for seven of these stars and infrared photometry for 16 of them and confirmed that many are carbon stars and apparent members of Fornax; their results were consistent with the assertion that *all* Fornax giants with $B - V \gtrsim 2.1$ are carbon stars. Since then Westerlund, Edvardsson, & Lundgren (1987, hereafter WEL) obtained grism plates of Fornax with the ESO 3.6 m telescope, and cataloged a total of 47 carbon stars, one S star, and 30 M stars in the Fornax field. Lundgren (1990) obtained spectrophotometry of 87 red stars in the direction of Fornax with the ESO 3.6 m telescope and the Faint Object Spectrograph and Camera and concluded that many of the noncarbon stars were not members of Fornax: he was able to identify only 15 M, MS, and S stars that appeared to be true members, while 10 appeared to be in the foreground. More recently, Azzopardi, Lequeux, & Muratorio (cited in Azzopardi & Lequeux 1992) catalog a total of 77 carbon stars in the Fornax field.

Figure 6 is a reproduction of our CMD for the bright red stars in the Fornax field. Solid circles represent our photometry for red stars identified by DK, while large and small crosses represent stars in our study but not noted by DK. In addition, we flag those stars with available spectroscopic classifications: five-pointed stars encompass the symbols denoting carbon stars and S stars as classified by WEL or Lundgren (1990), and large open circles surround points representing M stars, according to WEL or Lundgren. A few stars classified as "K" or "continuum" by Lundgren are not flagged. An additional carbon star, C12 in the numbering system of WEL, has an *R* magnitude near 18 but is not visible in a stack of nine of our *B*-band images. Since the *B*-band magnitude limit is greater than $B = 24$, this star must have had a $B - R$ color $\gtrsim$6 in mid-

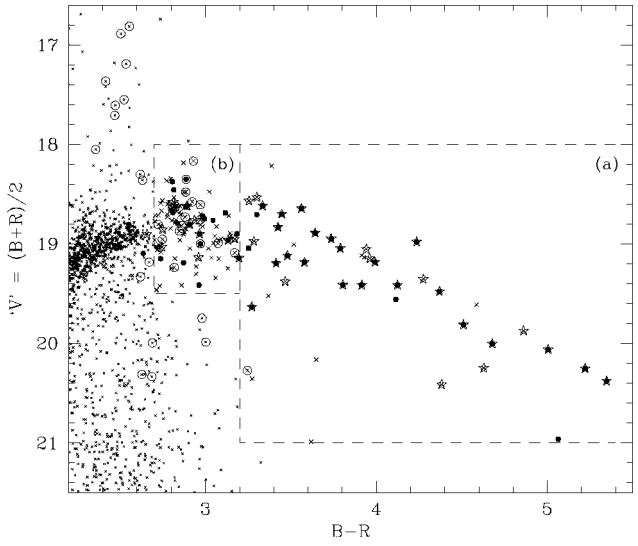

FIG. 6.—Expanded view of the giant-branch tip region of the CMD of the Fornax dwarf galaxy. Solid circles are stars appearing in the lists of red stars identified by Demers & Kunkel (1979). Large crosses represent red stars lying within the area of particular interest—delimited by the dashed lines and discussed in the text—that did not appear in the Demers & Kunkel list. Five-pointed stars flag spectroscopically confirmed carbon stars, and open circles indicate spectroscopically confirmed M stars from Westerlund et al. (1991) or Lundgren (1990).

December of 1995. In addition, star DK18 was measured to have $B = 24.90 \pm 0.30$ mag, $R = 18.440 \pm 0.007$ mag, whence "V" = 21.7 and $B - R = 6.5$, but because of the large uncertainty in the color it has not been plotted. Figure 6 shows that a significant fraction of the M stars in the Fornax field are either much brighter or much fainter than Fornax's giant branch at the same color and are likely to be foreground dwarfs, as argued by Lundgren.

For our present purposes, we pick out two classes of bright red stars that are likely to be true members of Fornax: class (a), those on the long, sloping tail to the red, with $18.00 <$ "V" < 21.00 and $B - R > 3.20$; and class (b), those in the detached patch of stars lying above and to the red of the normal giant branch, defined here as having $18.00 <$ "V" < 19.50 and $2.70 < B - R \leq 3.20$. These regions are outlined in Figure 6, and all stars meeting these criteria are listed in Table 1; unclassified stars within either of these two regions are denoted by the larger crosses in the figure. The coordinates given in the table are on a system defined by 119 stars with positions either in WEL or in the *Hubble Space Telescope* Guide Star Catalog. The standard deviation of the individual positional residuals was approximately 0.″9, so the coordinates given should be systematically correct to a few tenths of an arcsecond, and differentially precise to a few hundredths of an arcsecond. Alternative identifications in the naming schemes of DK and WEL are presented; none of the nine additional stars named by Lundgren (1990) falls into either of these categories of red star.[4] Carbon stars and S stars may be distinguished from M stars by (*a*) the letter "C," "M," or "S" incorporated into the DK or WEL star name in column (2) or (3)—these classifications are due to WEL—or (*b*) a spectral class given in the last column of the table; these are due to Lundgren. A single digit appearing in the last column indicates that a note is to be found at the end of the table. Considering the stars in Figure 6 that have spectroscopic classifications, it is clear that class (a) red stars are predominantly carbon stars, and class (b) contains a major admixture of M stars.

Table 1 contains three pairs of red stars with separations of 2.″5, 3.″0, and 5.″6, respectively. None of these six stars was included in the Demers & Kunkel list of red stars in Fornax, but one pair appears among the unclassified red stars in WEL's central Fornax field. Given that we have identified 161 candidate luminous red stars in an area of 1274 arcmin^2, we have a surface density of 0.13 candidates per square arcminute. The probability of finding a red star within 6″ of any given point is ~0.004, so the probability of finding one such pair among 161 stars is ~0.64, and the probability of finding three such pairs is ~0.26. Similarly, the probability of finding two pairs separated by less than 3″ is ~0.025. Therefore, it is possible that the stars in one or more of the pairs are physically related, which would imply that they are foreground main-sequence binaries, since it is unlikely that an extremely wide binary in Fornax would have both its components passing through the same brief evolutionary phase at the same time. One of the stars involved in the 3.″0 pair has a spectral type of S2/3 (according to Lundgren; this is star 65 in the current list [=WEL 34]), indicating that it, at least, is a probable member of Fornax. Lundgren states that his spectrum of the second star in this pair (star 64 = WEL 33) is "continuum," which means that the star is probably of spectral class G or early K. Our data indicate that the color of this star is similar to the colors of other stars that Lundgren classified as K5 or M, and even a few he classified as C or S. Regardless, the possibility that this alignment is purely fortuitous cannot be rejected. Even less can be said with confidence about the physical relationship of the other two red pairs.

3.3. Variable Stars

The way in which we obtained paired exposures in *B* and *R* at each visit to a particular subfield is optimum for exploiting the variable-finding technique of Welch & Stetson (1993; see Stetson 1996 for the particular variant of the technique employed here). Figure 7 shows the distribution of the modified Welch/Stetson variability index, *L*, as a function of pseudo-visual magnitude for all 82,183 Fornax stars observed in at least eight frame pairs. Note that this limit—imposed to maintain a reasonable signal-to-noise ratio in the variability in-

[4] From our visual examination we would judge that Lundgren 406 is a background galaxy.

TABLE 1
COORDINATES AND PHOTOMETRY FOR BRIGHT, RED STARS IN FORNAX

ID (1)	DK (2)	WEL (3)	R.A. (J2000) (4)	Decl. (J2000) (5)	B (6)	R (7)	"V" (8)	$B-R$ (9)	Note/Spectral Type (10)
1			02 38 07.77	−34 24 51.6	20.109 ± 0.215	17.258 ± 0.334	18.683	2.851	
2			02 38 12.81	−34 34 59.5	20.243 ± 0.049	17.447 ± 0.004	18.845	2.796	
3			02 38 17.11	−34 25 51.5	20.814 ± 0.021	17.682 ± 0.007	19.248	3.132	
4			02 38 39.18	−34 30 51.1	20.940 ± 0.636	17.973 ± 0.036	19.457	2.967	
5			02 38 40.14	−34 32 27.7	20.340 ± 0.007	17.467 ± 0.004	18.903	2.873	
6			02 38 47.19	−34 24 05.2	20.117 ± 0.005	17.339 ± 0.002	18.728	2.778	
7			02 38 50.94	−34 16 21.2	20.359 ± 0.011	17.293 ± 0.004	18.826	3.066	
8	32		02 38 51.55	−34 35 27.5	20.356 ± 0.005	17.055 ± 0.002	18.706	3.301	S2/5
9			02 38 56.48	−34 34 21.9	20.314 ± 0.005	17.611 ± 0.003	18.962	2.703	
10		M/30	02 38 58.23	−34 29 27.6	20.167 ± 0.009	17.443 ± 0.004	18.805	2.724	1
11	36C		02 38 58.28	−34 32 13.6	20.529 ± 0.009	17.397 ± 0.004	18.963	3.132	
12			02 39 00.30	−34 22 35.2	20.042 ± 0.010	17.191 ± 0.005	18.617	2.851	
13			02 39 05.63	−34 14 36.7	19.962 ± 0.009	17.223 ± 0.005	18.592	2.739	
14	31		02 39 05.64	−34 39 00.5	20.896 ± 0.014	17.933 ± 0.006	19.415	2.963	
15			02 39 08.09	−34 22 24.3	20.873 ± 0.027	17.813 ± 0.028	19.343	3.060	
16			02 39 08.11	−34 22 24.1	21.207 ± 0.032	17.838 ± 0.004	19.522	3.369	
17			02 39 08.62	−34 27 42.4	19.620 ± 0.003	16.748 ± 0.002	18.184	2.872	
18			02 39 10.72	−34 39 21.2	20.504 ± 0.034	17.427 ± 0.019	18.965	3.077	
19	40		02 39 11.26	−34 26 28.4	20.090 ± 0.004	17.282 ± 0.002	18.686	2.808	
20			02 39 12.00	−34 37 42.9	20.625 ± 0.009	17.753 ± 0.004	19.189	2.872	
21	35		02 39 12.49	−34 34 00.2	20.212 ± 0.005	17.229 ± 0.003	18.721	2.983	
22			02 39 14.42	−34 39 43.1	20.465 ± 0.008	17.320 ± 0.004	18.892	3.145	
23			02 39 15.32	−34 15 09.8	21.615 ± 0.019	17.500 ± 0.002	19.557	4.115	
24			02 39 15.78	−34 48 22.5	19.779 ± 0.026	16.972 ± 0.006	18.375	2.807	
25			02 39 16.78	−34 40 40.3	20.822 ± 0.012	18.109 ± 0.004	19.465	2.713	
26	34		02 39 17.65	−34 34 39.8	20.491 ± 0.006	17.306 ± 0.004	18.898	3.185	SC3/8
27		M2	02 39 20.68	−34 33 04.4	20.675 ± 0.008	17.504 ± 0.005	19.090	3.171	
28			02 39 21.32	−34 23 30.5	20.045 ± 0.012	17.194 ± 0.003	18.619	2.851	
29	38M		02 39 22.91	−34 28 11.1	20.485 ± 0.007	17.514 ± 0.004	19.000	2.971	
30		C15	02 39 23.36	−34 29 08.2	20.194 ± 0.006	16.939 ± 0.003	18.566	3.255	
31	31		02 39 24.17	−34 33 03.5	20.858 ± 0.013	17.378 ± 0.003	19.118	3.480	
32	29C		02 39 24.20	−34 38 04.1	20.064 ± 0.006	17.173 ± 0.005	18.618	2.891	
33			02 39 24.37	−34 32 54.4	19.940 ± 0.006	17.125 ± 0.003	18.533	2.815	
34			02 39 25.12	−34 27 29.6	19.751 ± 0.005	16.977 ± 0.005	18.364	2.774	
35	24M		02 39 25.32	−34 44 37.0	20.034 ± 0.006	17.209 ± 0.004	18.622	2.825	M1 S
36			02 39 25.75	−34 42 23.5	20.450 ± 0.010	17.395 ± 0.005	18.923	3.055	
37			02 39 26.45	−34 16 06.7	20.068 ± 0.009	17.362 ± 0.002	18.715	2.706	
38			02 39 26.73	−34 28 13.4	20.125 ± 0.004	17.421 ± 0.003	18.773	2.704	
39			02 39 29.82	−34 27 24.3	20.285 ± 0.006	17.148 ± 0.003	18.716	3.137	
40	41		02 39 30.63	−34 24 09.0	20.285 ± 0.013	17.241 ± 0.005	18.763	3.044	
41			02 39 31.43	−34 22 59.8	20.082 ± 0.007	17.271 ± 0.004	18.677	2.811	
42		C14	02 39 31.53	−34 31 52.1	19.986 ± 0.006	17.173 ± 0.005	18.580	2.813	
43	19C		02 39 31.75	−34 36 41.1	21.664 ± 0.026	17.294 ± 0.004	19.479	4.370	
44		M16	02 39 32.86	−34 17 03.8	19.920 ± 0.017	17.035 ± 0.006	18.478	2.885	M1 IV
45	28C		02 39 33.30	−34 38 31.4	20.258 ± 0.008	17.352 ± 0.003	18.805	2.906	
46	20C		02 39 34.37	−34 37 15.3	20.424 ± 0.013	16.862 ± 0.003	18.643	3.562	
47	17C		02 39 34.70	−34 38 58.8	21.270 ± 0.012	17.998 ± 0.003	19.634	3.272	
48		C18	02 39 36.68	−34 30 25.8	22.561 ± 0.186	17.932 ± 0.010	20.247	4.629	
49		C1	02 39 37.35	−34 36 28.0	22.565 ± 0.041	17.559 ± 0.004	20.062	5.006	
50			02 39 37.49	−34 25 01.2	19.743 ± 0.006	16.945 ± 0.003	18.344	2.798	
51			02 39 37.52	−34 35 16.1	20.092 ± 0.006	17.314 ± 0.003	18.703	2.778	
52		M12	02 39 39.00	−34 32 22.1	20.245 ± 0.008	17.385 ± 0.004	18.815	2.860	
53	42C		02 39 39.40	−34 24 58.9	20.974 ± 0.011	17.394 ± 0.003	19.184	3.580	
54		14	02 39 39.43	−34 28 47.9	19.632 ± 0.006	16.702 ± 0.004	18.167	2.930	M2 S
55	47C		02 39 39.63	−34 19 53.3	20.545 ± 0.007	17.120 ± 0.002	18.833	3.425	

TABLE 1
(Continued)

ID (1)	DK (2)	WEL (3)	R.A. (J2000) (4)	Decl. (J2000) (5)	B (6)	R (7)	"V" (8)	$B-R$ (9)	Note/Spectral Type (10)
56			02 39 40.08	−34 34 03.4	20.039 ± 0.010	17.295 ± 0.006	18.667	2.744	
57	46C		02 39 40.58	−34 20 15.8	21.097 ± 0.010	16.861 ± 0.002	18.979	4.236	
58			02 39 40.89	−34 33 00.0	20.071 ± 0.009	17.346 ± 0.003	18.708	2.725	2
59			02 39 40.91	−34 32 57.5	20.071 ± 0.008	17.195 ± 0.006	18.633	2.876	2
60			02 39 41.36	−34 22 52.1	20.391 ± 0.009	17.673 ± 0.003	19.032	2.718	
61		C3	02 39 41.51	−34 33 41.5	21.111 ± 0.016	17.644 ± 0.004	19.377	3.467	3
62			02 39 43.33	−34 13 49.7	20.193 ± 0.008	17.368 ± 0.002	18.781	2.825	
63			02 39 44.05	−34 26 11.1	20.074 ± 0.007	17.197 ± 0.003	18.635	2.877	
64		33	02 39 44.47	−34 28 55.0	19.938 ± 0.006	17.190 ± 0.006	18.564	2.748	2, ctm
65		34	02 39 44.69	−34 28 56.3	20.495 ± 0.007	17.405 ± 0.007	18.950	3.090	2, S2/3
66	27M		02 39 44.82	−34 38 58.4	19.794 ± 0.006	16.907 ± 0.003	18.351	2.887	M2 S
67			02 39 45.02	−34 40 12.5	20.453 ± 0.010	17.714 ± 0.004	19.083	2.739	
68			02 39 45.14	−34 19 34.1	20.384 ± 0.018	17.675 ± 0.013	19.029	2.709	
69			02 39 48.41	−34 35 08.8	21.905 ± 0.082	17.319 ± 0.002	19.612	4.586	
70	37C		02 39 49.13	−34 31 24.8	20.284 ± 0.016	16.949 ± 0.004	18.617	3.335	
71		58	02 39 49.76	−34 27 31.5	20.055 ± 0.005	17.257 ± 0.006	18.656	2.798	K5
72			02 39 51.41	−34 39 13.7	19.990 ± 0.010	17.210 ± 0.003	18.600	2.780	
73			02 39 51.75	−34 17 18.3	20.186 ± 0.009	17.214 ± 0.005	18.700	2.972	2
74		C5	02 39 51.82	−34 33 21.0	23.656 ± 0.103	17.577 ± 0.004	20.617	6.079	
75			02 39 51.96	−34 17 13.3	20.043 ± 0.006	17.248 ± 0.003	18.646	2.795	2
76	10C		02 39 53.27	−34 46 03.9	20.383 ± 0.017	17.417 ± 0.018	18.900	2.966	
77			02 39 53.84	−34 44 04.0	23.495 ± 0.136	18.430 ± 0.008	20.963	5.065	
78		C4	02 39 53.94	−34 34 25.3	20.181 ± 0.015	16.880 ± 0.003	18.530	3.301	
79			02 39 53.96	−34 42 12.3	20.291 ± 0.008	17.404 ± 0.004	18.847	2.887	
80	43C		02 39 54.59	−34 22 43.6	20.711 ± 0.013	17.069 ± 0.003	18.890	3.642	
81		M17	02 39 54.89	−34 21 02.3	21.896 ± 0.016	18.650 ± 0.003	20.273	3.246	
82		C13	02 39 55.17	−34 25 27.4	21.024 ± 0.011	17.082 ± 0.004	19.053	3.942	
83			02 39 56.15	−34 25 23.2	20.374 ± 0.008	17.647 ± 0.004	19.010	2.727	
84		86	02 39 57.17	−34 36 09.6	20.038 ± 0.008	17.115 ± 0.003	18.576	2.923	M1 S
85		91	02 39 57.93	−34 35 49.6	20.039 ± 0.008	17.234 ± 0.003	18.636	2.805	M1
86	22C	93	02 39 58.32	−34 36 22.5	20.939 ± 0.008	17.149 ± 0.004	19.044	3.790	C3,3
87		M11	02 39 58.58	−34 25 28.9	20.242 ± 0.005	17.272 ± 0.003	18.757	2.970	M2 S
88			02 39 59.47	−34 32 44.2	19.917 ± 0.006	17.043 ± 0.003	18.480	2.874	
89	44C		02 40 00.90	−34 22 44.2	21.179 ± 0.016	17.187 ± 0.003	19.183	3.992	
90	48C		02 40 01.32	−34 20 19.8	21.371 ± 0.016	17.456 ± 0.002	19.413	3.915	
91			02 40 01.78	−34 44 05.1	20.212 ± 0.007	17.375 ± 0.005	18.793	2.837	
92	55C		02 40 02.48	−34 27 43.5	23.053 ± 0.088	17.705 ± 0.006	20.379	5.348	
93	5C		02 40 02.67	−34 48 27.2	20.741 ± 0.011	17.545 ± 0.005	19.143	3.196	
94	62C		02 40 02.69	−34 31 49.8	22.864 ± 0.060	17.642 ± 0.004	20.253	5.222	
95		M27	02 40 04.06	−34 45 15.8	20.295 ± 0.019	17.447 ± 0.013	18.871	2.848	
96			02 40 04.11	−34 20 11.7	20.493 ± 0.005	17.344 ± 0.003	18.918	3.149	
97	64C		02 40 04.31	−34 34 40.6	20.423 ± 0.051	16.976 ± 0.006	18.700	3.447	
98	61C		02 40 05.33	−34 32 19.1	22.067 ± 0.027	17.557 ± 0.004	19.812	4.510	
99	54S		02 40 05.49	−34 27 44.1	21.314 ± 0.011	17.510 ± 0.007	19.412	3.804	S4/5
100		C6	02 40 06.13	−34 35 28.6	20.229 ± 0.011	17.293 ± 0.007	18.761	2.936	4
101			02 40 06.46	−34 20 14.1	20.387 ± 0.009	17.536 ± 0.009	18.961	2.851	
102		C11	02 40 07.84	−34 30 15.1	20.536 ± 0.010	17.364 ± 0.004	18.950	3.172	
103			02 40 08.14	−34 26 06.5	19.988 ± 0.006	16.964 ± 0.008	18.476	3.024	
104		C7	02 40 09.05	−34 34 40.7	21.491 ± 0.025	17.216 ± 0.005	19.354	4.275	
105		C10	02 40 10.12	−34 33 22.8	22.305 ± 0.032	17.443 ± 0.008	19.874	4.862	
106		145	02 40 10.99	−34 33 01.5	20.230 ± 0.005	17.480 ± 0.003	18.855	2.750	S1/6
107		143	02 40 11.56	−34 27 53.2	20.405 ± 0.009	17.659 ± 0.003	19.032	2.746	C2,2
108	60C	149	02 40 11.74	−34 32 46.4	20.817 ± 0.014	17.081 ± 0.004	18.949	3.736	C3,2
109	59C		02 40 12.19	−34 30 10.2	20.900 ± 0.009	17.487 ± 0.003	19.194	3.413	
110			02 40 12.43	−34 39 06.9	20.499 ± 0.008	17.533 ± 0.005	19.016	2.966	

TABLE 1
(Continued)

ID (1)	DK (2)	WEL (3)	R.A. (J2000) (4)	Decl. (J2000) (5)	B (6)	R (7)	"V" (8)	$B-R$ (9)	Note/Spectral Type (10)
111			02 40 13.64	−34 43 24.0	19.864 ± 0.007	17.049 ± 0.005	18.457	2.815	
112			02 40 13.99	−34 23 32.5	20.086 ± 0.007	17.184 ± 0.004	18.635	2.902	
113		M3	02 40 14.33	−34 34 13.2	20.172 ± 0.006	17.290 ± 0.005	18.731	2.882	5
114		M7	02 40 14.49	−34 30 42.0	20.091 ± 0.009	17.121 ± 0.005	18.606	2.970	M
115	65C		02 40 15.57	−34 34 04.0	22.343 ± 0.050	17.664 ± 0.006	20.003	4.679	
116	49		02 40 17.05	−34 22 12.8	20.246 ± 0.013	17.129 ± 0.006	18.688	3.117	SC4/8
117		175	02 40 18.26	−34 34 48.2	20.646 ± 0.025	17.828 ± 0.009	19.237	2.818	M1
118			02 40 18.39	−34 38 30.9	20.646 ± 0.014	17.845 ± 0.005	19.245	2.801	
119		M19	02 40 18.98	−34 18 47.5	20.516 ± 0.006	17.468 ± 0.004	18.992	3.048	S3/2
120		M4	02 40 19.54	−34 32 54.3	20.328 ± 0.009	17.579 ± 0.005	18.953	2.749	M
121			02 40 19.79	−34 07 56.3	22.798 ± 0.071	19.179 ± 0.014	20.989	3.619	
122		C9	02 40 19.89	−34 33 10.9	22.605 ± 0.040	18.223 ± 0.006	20.414	4.382	
123		C8	02 40 20.32	−34 34 56.0	20.616 ± 0.013	17.656 ± 0.008	19.136	2.960	6
124			02 40 22.63	−34 40 38.5	20.106 ± 0.012	17.255 ± 0.004	18.681	2.851	
125		C17	02 40 23.37	−34 43 24.0	21.127 ± 0.013	17.165 ± 0.005	19.146	3.962	
126			02 40 23.47	−34 15 21.3	20.165 ± 0.009	17.361 ± 0.007	18.763	2.804	
127			02 40 23.83	−34 18 11.8	20.132 ± 0.007	17.276 ± 0.003	18.704	2.856	
128			02 40 24.06	−34 40 58.5	20.219 ± 0.009	17.377 ± 0.004	18.798	2.842	
129		C16	02 40 24.09	−34 34 19.4	20.615 ± 0.024	17.331 ± 0.003	18.973	3.284	7
130		M22	02 40 24.41	−34 10 42.2	20.531 ± 0.052	17.457 ± 0.008	18.994	3.074	
131	56C		02 40 24.98	−34 28 59.4	21.476 ± 0.010	17.352 ± 0.003	19.414	4.124	
132	50		02 40 25.26	−34 20 42.2	20.517 ± 0.005	17.779 ± 0.003	19.148	2.738	SC2/8
133			02 40 25.30	−34 30 14.6	20.387 ± 0.011	17.648 ± 0.004	19.017	2.739	
134			02 40 31.87	−34 20 49.7	20.499 ± 0.011	17.590 ± 0.006	19.045	2.909	
135			02 40 32.81	−34 39 22.0	20.420 ± 0.010	17.702 ± 0.007	19.061	2.718	
136			02 40 34.06	−34 23 51.4	20.669 ± 0.007	17.416 ± 0.002	19.042	3.253	
137			02 40 36.60	−34 17 14.6	20.292 ± 0.007	17.320 ± 0.007	18.806	2.972	
138			02 40 38.98	−34 26 47.3	20.186 ± 0.005	17.448 ± 0.002	18.817	2.738	
139			02 40 39.51	−34 36 10.9	20.089 ± 0.006	17.258 ± 0.004	18.674	2.831	
140	58		02 40 39.77	−34 31 34.4	20.247 ± 0.007	17.253 ± 0.002	18.750	2.994	
141			02 40 39.97	−34 29 38.3	20.262 ± 0.005	17.349 ± 0.003	18.806	2.913	
142			02 40 40.09	−34 28 46.6	20.819 ± 0.007	18.104 ± 0.005	19.462	2.715	
143			02 40 41.00	−34 23 56.1	20.553 ± 0.009	17.535 ± 0.004	19.044	3.018	
144			02 40 48.32	−34 35 38.0	19.910 ± 0.006	16.523 ± 0.004	18.216	3.387	
145			02 40 48.62	−34 30 54.5	20.700 ± 0.009	17.754 ± 0.004	19.227	2.946	
146			02 40 49.90	−34 31 12.9	20.558 ± 0.008	17.737 ± 0.002	19.147	2.821	
147			02 40 49.94	−34 25 59.4	20.765 ± 0.008	17.247 ± 0.004	19.006	3.518	
148			02 40 52.16	−34 37 24.8	21.071 ± 0.019	17.157 ± 0.006	19.114	3.914	
149			02 40 55.27	−34 27 26.7	20.174 ± 0.006	17.346 ± 0.006	18.760	2.828	
150			02 40 56.77	−34 27 10.8	19.972 ± 0.009	17.187 ± 0.005	18.580	2.785	
151			02 41 05.82	−34 27 33.3	20.317 ± 0.017	17.333 ± 0.008	18.825	2.984	
152			02 41 08.21	−34 35 54.3	21.100 ± 0.015	17.172 ± 0.004	19.136	3.928	
153			02 41 10.73	−34 31 53.4	20.324 ± 0.018	17.446 ± 0.003	18.885	2.878	
154			02 41 16.79	−34 25 22.4	20.788 ± 0.008	18.055 ± 0.005	19.422	2.733	
155			02 41 19.71	−34 25 44.4	20.061 ± 0.007	17.173 ± 0.003	18.617	2.888	
156			02 41 20.00	−34 30 37.3	20.775 ± 0.011	17.830 ± 0.004	19.302	2.945	
157			02 41 20.70	−34 24 00.9	20.657 ± 0.029	17.621 ± 0.005	19.139	3.036	
158			02 41 26.87	−34 22 09.6	20.846 ± 0.059	17.986 ± 0.022	19.416	2.860	
159			02 41 26.90	−34 22 08.8	21.988 ± 0.101	18.339 ± 0.027	20.164	3.649	
160			02 41 28.35	−34 23 24.9	21.993 ± 0.053	18.719 ± 0.047	20.356	3.274	
161			02 41 32.29	−34 22 58.1	20.688 ± 0.127	17.609 ± 0.031	19.148	3.079	

NOTES.—Units of right ascension are hours, minutes, and seconds, and units of declination are degrees, arcminutes, and arcseconds. (1) Star 30 in the unpublished list of Blanco & McCarthy; see Frogel et al. 1982. (2) Member of a close pair of bright red stars. (3) The coordinates given by WEL appear to contain a typographical error. The star listed here is the one marked in their finding chart. Its coordinates, precessed back to 1950.0, are $02^h37^m37\overset{s}{.}3$, $-34°4'$, while WEL give $02^h37^m41\overset{s}{.}2$, $-34°46'33''$. (4) =WEL 126. (5) =WEL 157. (6) =WEL 187. (7) =WEL 202.

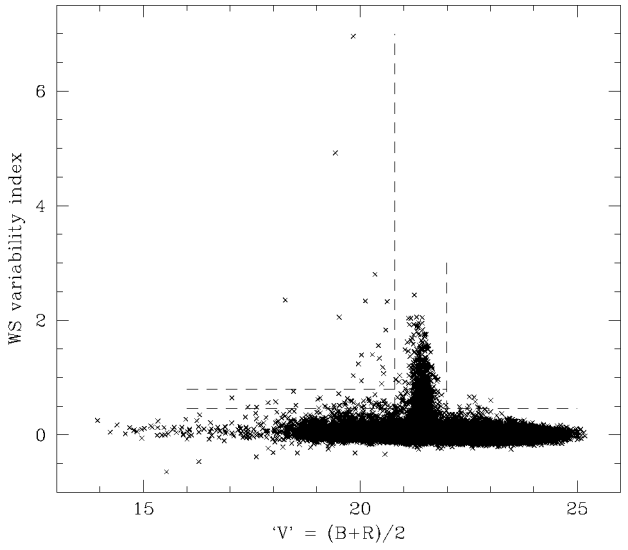

FIG. 7.—Plot of the modified Welch/Stetson variability index L vs. magnitude for stars in the Fornax field that were measured in at least eight frame pairs. Dashed lines delimit the regions occupied by probable variables in five categories, as discussed in the text.

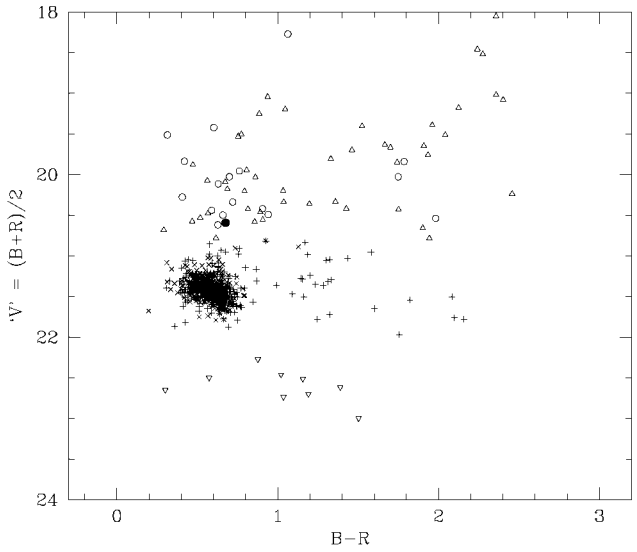

FIG. 8.—CMD for candidate short-period variable stars in the field of the Fornax dwarf galaxy. Crosses represent highly probable RR Lyrae stars; plusses represent probable RR Lyraes; open circles represent highly probable variables brighter than the horizontal branch; upward-pointing triangles represent probable luminous variables; and downward-pointing triangles represent probable variables fainter than the horizontal branch. A single filled circle represents the probable anomalous Cepheid cluster 3 star 76, previously identified by Light et al. (1986).

dex—excludes the outer halves of the north, east, south, and west subfields, and the outer quadrants of the northeast, southeast, southwest, and northwest subfields. Counting pixels as before, we find that almost exactly half of the survey area, 637 arcmin^2, is contained within at least eight frame pairs. Among the stars included in this restricted sample, the average value of L was 0.028, and the standard deviation was 0.109. In the discussion that follows, we will adopt as candidate variables those stars with $L > 0.46$; this corresponds to a one-sided significance level of 4.0 $\sigma \Rightarrow$ a cumulative probability of 0.99997, indicating that we would expect roughly three false positive detections per 100,000 stars if L obeys a Gaussian probability distribution. Unfortunately, our observing pattern—5 hr of intermittent (for any one portion of the field) coverage at 1 day intervals spanning a total of slightly over three days—was not optimal for deriving unique phased light curves for variables whose periods most likely lie in the range 0.25–0.8 days and, indeed, our attempts to derive such light curves have not met much success. Therefore, our interpretation of the physical nature of the variable candidates will rely on cruder photometric diagnostics. Among the 30 long-period variables in Fornax cataloged by Demers & Irwin (1987), 19 fell within our survey area and 12 appeared in at least eight frame pairs; as would be expected, none met our variability criteria. Of the two short-period variables identified by Light, Armandroff, & Zinn (1986), one—cluster 3 star 76 (Buonanno et al. 1985)—fell within our survey area; it had $L = 1.829$ and is thus recovered as a highly probable variable star.

Dashed lines in Figure 7 divide the candidate variables into five categories. The prominent pillar of points around "V" $\sim$ 21.5 is obviously dominated by RR Lyrae variables in Fornax, so stars in the range $20.8 <$ "V" < 22.0 have been divided into (*a*) 298 highly probable variables with $L > 0.8$, and (*b*) 326 probable variables with $0.46 < L \leq 0.8$. The 298 highly probable RR Lyraes have unweighted mean magnitudes $\langle B \rangle = 21.68$, $\langle R \rangle = 21.11$, while the full sample of 624 candidates has $\langle B \rangle = 21.71$, $\langle R \rangle = 21.10$. Candidate variables brighter than "V" $= 20.8$ have been similarly divided into (*c*) 18 highly probable variables and (*d*) 50 probable variables, again with the dividing line at $L = 0.8$. Finally, fainter than "V" $= 22.0$ there are (*e*) nine probable variables with $L > 0.46$. Figure 8 shows these five categories of candidate variable star plotted in a CMD. Here we see that the vast majority of the candidate RR Lyrae variables (*crosses and plusses*) are indeed concentrated in the area of the instability strip (compare Fig. 4, which is plotted to the same scale). A few candidate RR Lyraes tail off toward Fornax's giant branch, but these tend to be the merely probable RR Lyraes (*plusses*) rather than the highly probable ones (*crosses*): only one of the 298 highly probable variables lies redward of $B - R = 1.00$, whereas 23 of the 326 probable variables are found there. These redder RR Lyrae candidates could be (1) RR Lyraes accidentally caught in the reddest phases of their cycle (there would be fewer anomalously blue candidates because RR Lyraes spend the greatest fraction of their time near the red extreme of their color range), (2) RR Lyraes blended with redder stars (the lack of anomalously blue candidates being due to a shortage of blue stars to be blended

with), (3) nonvariable clump stars or giants for which non-Gaussian errors have produced a positive value of L, and/or (4) something else.

Among the brighter variables, the open circles, upward-pointing triangles, and one filled circle for cluster 3 star 76, there are concentrations in the area above the horizontal branch and in the region of the giant branch. The former are likely to be anomalous Cepheids of the type commonly found in dwarf spheroidal galaxies and include most of the highly probable candidates: 15 of the 17 open circles and the filled circle are found to the blue of $B - R = 1.40$, as are 30 of the 50 triangles. The redder bright variable candidates are more of a mystery: with data spanning a total time range of 3.19 days, it is hardly likely that we could have detected a large fraction of any W Virginis, Cepheid, or semiregular giant variables in Fornax unless there are very many of them and we caught the ones with the shortest periods and those that happened to be at rising light. Again, it is possible that these stars are blends of bluer variables with red, constant stars, or that some of them have been promoted to candidate variable status by non-Gaussian errors.

It is tempting to postulate that the fainter variables, the nine downward-pointing triangles, are W Ursae Majoris–type eclipsing main-sequence binaries, and this identification may in fact be correct. But with a broad color distribution across the bottom of the CMD, it is unlikely that any but the bluest one or two could be spectral class A or F main-sequence stars in Fornax; instead, it would seem that most must be G-, K-, or M-type main-sequence eclipsing binaries in the foreground population. This possibility might also be the true explanation for at least some of the bright red variables, particularly the reddest plusses and the three highly probable open circles near "V" $\sim$ 20, $B - R \sim 1.9$.

3.4. Overall Spatial Distribution

Hodge (1961b) counted 60,000 stars in 170 arcsec^2 cells spanning some 15,000 arcmin^2 in four ADH Schmidt plates of the Fornax dwarf galaxy. He found that the galaxy was highly elongated in the northeast-southwest direction (major-axis position angle 54°), with ellipticity $\epsilon = 1 - (b/a)$ ranging from $\sim$0.2 near the center to $\sim$0.35 for the outer isopleths. Hodge also noted a significant asymmetry in the star counts parallel to the major axis, in the sense that the maximum surface density appeared to occur some 6′ northeast of the centroid of the outermost isopleths. A similar, though smaller, asymmetry was found in the stellar distribution parallel to the minor axis. As the canon at the time held that the dwarf spheroidal galaxies were the littlest ellipticals or, equivalently, the biggest globular clusters, each of which class of object was held to consist of a single generation of stars characterized by ellipsoidal geometric and kinematic distributions, this asymmetry was surprising. Even though the two-body relaxation time would be prohibitively long in an entity with as low a spatial stellar density as Fornax, any asymmetries obtaining in the initial conditions at the galaxy's birth should have been erased in a few crossing times (it being implicitly assumed that all Fornax comprised a single kinematic population). One possibility was that an extensive though diffuse dust cloud in Fornax might be suppressing the star counts at and to one side of the true position of maximum stellar density.

Demers et al. (1994) revisited the question of the stellar density distribution in Fornax, utilizing APM scans of four plates from the prime focus of the Cerro Tololo 4 m telescope. They considered counts of some 52,000 stellar-appearing images in two circular fields, each roughly 46′ in diameter, one centered roughly 10′ southwest of the center of Fornax, the other about 20′ north of the center. They confirmed the asymmetry of the major-axis profile in Fornax, although a quantitative description of that asymmetry was hampered by the truncation of the northeast quadrant of the galaxy by vignetting in their plates. By numerically fitting ellipses to their observed star counts in 36″ cells, Demers et al. concluded (*a*) that the centroids of the innermost isopleths are displaced to the northeast of the centroids of the outermost ones, (*b*) that the surface density of stars in Fornax peaks at the position of globular cluster 4, and (*c*) that the ellipticity and position angle change erratically from one isopleth to the next in the "chaotic inner parts" of Fornax. In the course of analyzing their CMD, Demers et al. looked for—and failed to find—any signature of the dust that Hodge (1961b) postulated to explain the asymmetry in Fornax's star-count profile.

Figure 9 is a gray-scale rendering of our counts of all stars with $18.5 <$ "V" < 23.0 in 30″ cells; the reader may orient this map in comparison to Figure 1 by recognizing globular cluster 3 north (*to the right*) of the main body of the galaxy, and the hole in the star counts produced by the bright star HD 16690 west of (*above*) the center of the galaxy. Seen in this way, Fornax does present an *azimuthally* asymmetric appearance, with a boomerang-shaped ridge of star density lying around the galactic center on the north and east sides, and a somewhat more diffuse fog of stellar density spreading to the southwest. This appearance should not be an artifact of a variable magnitude limit: our star counts should be essentially complete to well below magnitude 23 in the entire survey area. Crowding should not be a problem even near the center of the galaxy (except, of course, in the two globular clusters), and if crowding were a factor, it would not be expected to create an apparent azimuthal asymmetry where none existed in reality. However, we note that the star counts in Fornax tend to show considerable *bilateral* symmetry about an axis lying in a northeast-southwest (*bottom right to top left*) direction. It will be interesting to learn whether this symmetry axis happens to lie in the direction of Fornax's orbit about the Galaxy, when proper motions eventually become available. It is possible that the "chaotic" nature of the center of Fornax, as described by Demers et al., is not real, but rather results from a failure of the assumption of elliptical symmetry: given the Poisson noise of star counts in

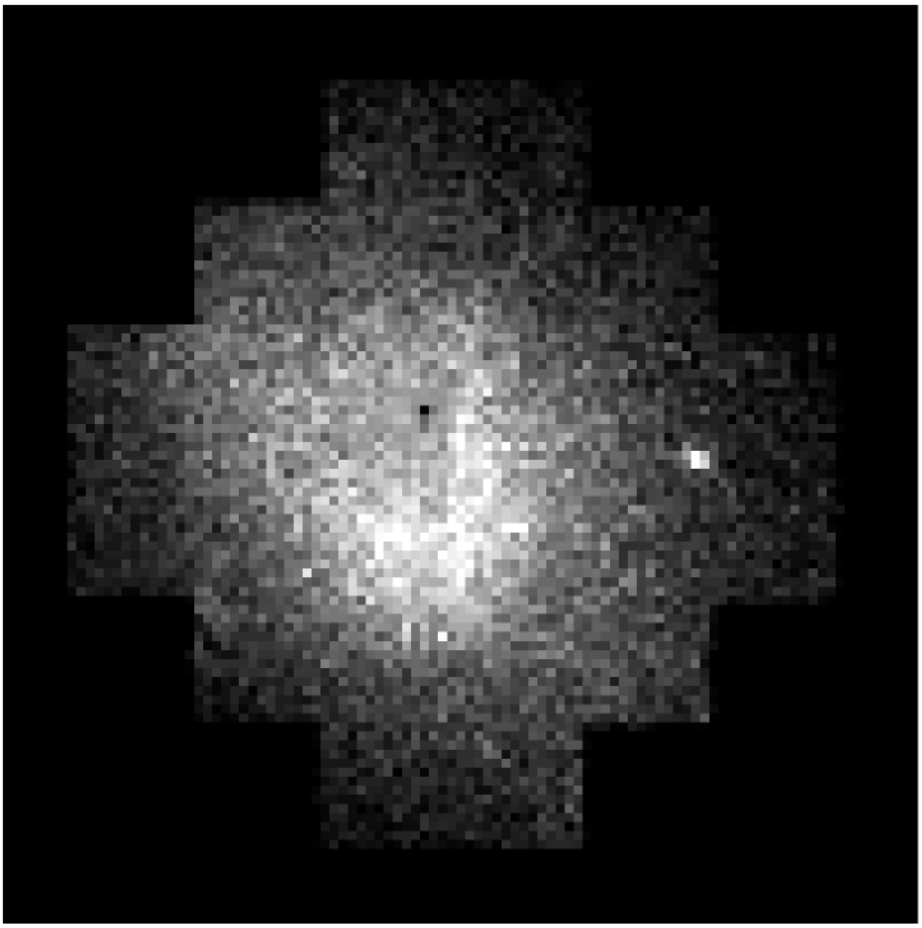

FIG. 9.—Gray-scale plot of the stellar surface density in 30″ cells in the field of the Fornax dwarf galaxy. Only stars with $18.5 < \text{“}V\text{”} < 23$ have been counted, and a brighter tone represents a higher density of stars. Orientation is the same as Fig. 1: north to the right and west up.

small projected cells, plus the freedom to choose the ellipticity, position angle, and centroid of each successive elliptical isopleth, it is little wonder that Demers et al. observed erratic behavior in their fitted ellipses as the “centroid” of Fornax was approached.

We have tried to render this distribution of stars as a contour plot using a standard package, without noteworthy success. The signal-to-noise ratio in this “image” is comparatively low: 82,183 stars are divided among 4980 quarter-square-arcminute cells, for an average of 16.5 stars per cell and a typical signal-to-noise ratio of 4. As a result, the contour plot is very noisy, and some contours do not close on themselves. A simple-minded smoothing scheme could be applied, but it would mix in the zeros from the L-shaped corners of the image where there are no data, and—whether the data were smoothed or not—standard contouring packages would place the outermost isopleths parallel to the edges of the zones where data are missing, whereas an ideal package would allow the isopleths to intersect the regions of missing data at arbitrary angles. A custom contouring scheme could—and probably should—be written to deal with the case of arbitrarily censored data such as we have here, but it does not seem worth the effort for our present purposes.

Instead, we adopted a much cruder scheme to demonstrate and quantify the asymmetry of Fornax’s profile. A global centroid of Fornax in the plane of the sky was estimated by allowing a circular aperture of radius 2000 pixels = 14.′5 to wander over our table of positions and photometry until the median (x, y) position of all stars with $18.5 < \text{“}V\text{”} < 23.0$ contained within the aperture coincided with the position of its center. This condition was satisfied with the circle centered at pixel coordinates (794, 861), corresponding to $\alpha_{2000} = 02^{h}39^{m}54.^{s}6$, $\delta_{2000} = -34°30'44''$ (equinox 2000.0). For comparison, Hodge & Smith (1974) obtained a Fornax centroid of $02^{h}39^{m}52^{s}$, $-34°31.'6$ (2000.0) from an average of estimates from their five plates, and the machine-weighted center of gravity of Fornax based upon APM scans reported by Demers & Irwin (1987) was $02^{h}39^{m}53.^{s}1$, $-34°30'16''$ (2000.0). Then our centroiding exercise was repeated with circles of radius 1500, 1000, and 500 pixels. Their centroids in pixel units came out

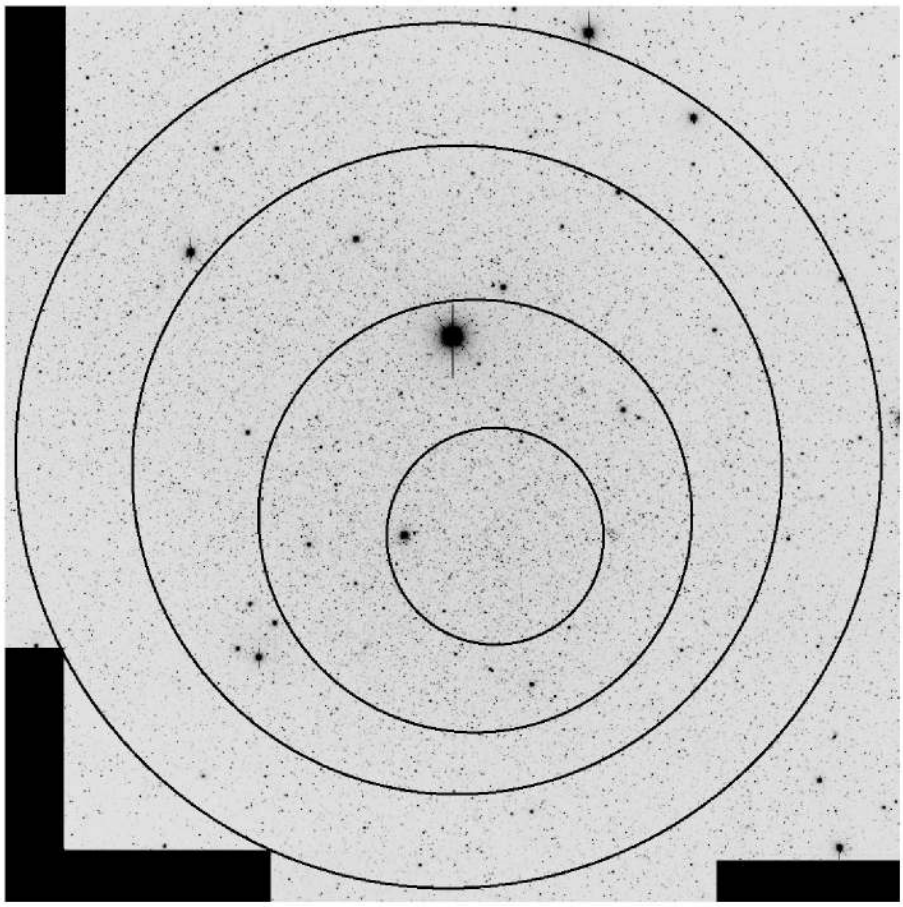

FIG. 10.—Enlargement of the central part of the survey area, showing the 2000, 1500, 1000, and 500 pixel circles used to estimate the positions of peak stellar density. Each circle has been placed so that its center coincides with the median (x, y) coordinates of the stars contained within it. As the surface-density peak of the Fornax galaxy is more and more narrowly defined, it moves farther and farther to the northeast.

to (833, 796), (917, 582), and (1010, 488), based on 43,387, 23,286, and 6884 stars, respectively. The centroid of the 500 pixel circle lies at $\alpha_{500} = 02^h40^m07\overset{s}{.}7$, $\delta_{500} = -34°29'10''$ (2000.0), which is 1′.57 north and 2′.70 east of the centroid of the 2000 pixel circle; the position angle defined by these two points is 60° east of north. As these numbers and Figure 10 show, as the peak of the stellar density distribution in Fornax is more and more narrowly defined, that peak is displaced farther and farther to the northeast. Notice particularly in Figure 10 that, except for just a very few pixels in the south-southeast part of the 2000 pixel circle, each region considered falls entirely within the survey area and avoids the populous globular cluster 3 north of the center of the galaxy, but not the fainter globular cluster 4 east-southeast of the center. The use of the median rather than the mean position of the stars contained in each circle reduces the systematic effect of the presence of this globular cluster and the zone of avoidance produced by the saturated image of HD 16690 some 4′.0 west of the center of the galaxy. However, if the cluster and the hole produced by the bright star *were* to affect the results of this analysis, both would act in the sense of biasing the three *largest* circles toward the *east* and the *smallest* circle toward the *south*, which is contrary to what we observe. Therefore, we agree with the previous researchers that the asymmetry in Fornax's profile is probably real. Our estimate of the position of the peak density in Fornax, as given by the centroid of the 500 pixel circle, lies some 0′.5 west and 2′.5 north of cluster 4 (whose position is $02^h40^m10^s$, $-34°31'34''$ [2000.0] according to Hodge & Smith). This is similar to the estimates of Hodge (1961b) and Hodge & Smith (1974), but distinct from the claim of Demers & Irwin, who said that the peak of Fornax coincides with cluster 4.

3.5. Spatial Distribution of Subpopulations

It is of interest to ascertain whether the oldest and younger generations of stars in Fornax occupy the same volume, or whether one population is laterally displaced or more radially concentrated in comparison to another. With only the data in hand it is clearly not possible to associate each individual star with an age, a chemical abundance, or a kinematic distribution.

However, for purposes of the present discussion, we will assume that common belief is in fact truth, and that the candidate RR Lyrae variables can serve as a suitable proxy for the oldest, most metal-poor stars in Fornax; that the quasi-circular red horizontal branch clump (excluding the fainter, extended red horizontal branch) suitably represents an intermediate-age, more metal-rich population; and that the plume of blue stars represents a very young population. In this context, the population status of the two classes of red giant more luminous than the standard giant-branch tip is not immediately obvious. Therefore, stars were selected that met the following criteria. First, for consistency with the constraints on the RR Lyrae candidates, all stars must have appeared in a minimum of eight frame pairs. Then, we define RR Lyraes as having $L > 0.46$, $20.80 < \text{“}V\text{”} < 22.00$, $0.00 < B - R < 1.00$; clump stars have no limit on L, $21.00 < \text{“}V\text{”} < 21.60$, $1.05 < B - R < 1.25$; blue stars have no limit on L, $18.50 < \text{“}V\text{”} < 22.00$, $B - R < 0.25$; red stars (class [a]) have no limit on L, $18.00 < \text{“}V\text{”} < 21.00$, $B - R > 3.20$; red stars (class [b]) have no limit on L, $18.00 < \text{“}V\text{”} < 19.50$, $2.70 < B - R \leq 3.20$.

Finally, we defined the set of “all” Fornax stars in at least eight frame pairs, with $18.50 < \text{“}V\text{”} < 23.00$ and $B - R < 1.70 + 0.8125(23.00 - \text{“}V\text{”})^2$ [defining a horizontal parabola with a vertex at $(B - R, \text{“}V\text{”}) = (1.70, 23.00)$ and passing through (3.00, 19.00)], to exclude as many as possible of the apparent foreground dwarfs. The reader is invited to apply a ruler to Figures 3, 4, and 5.

Each of these population proxies will show some net displacement from the Fornax centroid that we adopted above, because the region of sky that was contained within eight frame pairs is not symmetric about that centroid. However, since the same areal constraint was placed on all five samples, any global difference in their distributions should still be reflected in relative comparisons between samples. The exact size and direction of such differences will not be *exactly* reproduced within this odd polygonal subsample of Fornax, but the displacements seen should at least be in the correct sense and of the right order of magnitude.

Mean net offsets and rms distances from the Fornax density peak (as defined by the 500 pixel circle discussed above) for each of the five samples are given in Table 2. Here we see that the location and extent of the intermediate-age, putatively metal-rich population represented by 7969 “clump” stars is practically identical to the location and extent of the total Fornax sample. This is reasonable, since the strength of the clump and the redmost giant branch in the CMD suggests strongly that this population dominates at least the central part of the galaxy. It appears that the old, metal-poor population—as defined by its RR Lyrae proxies—is centered some 90″ north ($+x$) and 30″ west ($+y$) of the main body of Fornax and is some 13% more radially extended. Conversely, the blue stars apparently defining a very young main sequence are centered some 30″ north and 15″ west of the intermediate-age population and are only 88% as extended on the sky. According to the central-limit theorem, the confidence level that can be placed on these statements is of the order of magnitude rms radius divided by $\sqrt{N}$ (more rigorous statistical analysis is hardly relevant given the state of the data): e.g., $\pm 657''/\sqrt{600} = \pm 27''$ for the RR Lyrae sample—so their net displacement with respect to “all” Fornax stars appears to be a 3.6 σ effect—and 12.″5 for the blue-star sample, so their net displacement is significant at the 2.8 σ level. Similarly, the difference between the rms radii for the clump and blue stars, 594″ versus 521″, is significant at a 4.8 σ level. The data for the red stars are consistent with class (a) extremely red giants being of the same centrally concentrated population as the blue stars, while the class (b) very red giants more closely resemble the intermediate-age clump stars in their spatial extent. However, due to the extremely small sample sizes, the difference between a mean radius of 509″ and 600″—while suggestive—is significant at only the ~1 σ level.

Figure 11 reveals the actual distribution over our survey area of each of the four subpopulations defined above. The solid lines represent the boundaries of the region defined by a minimum of eight frame pairs, and (0, 0) on the graph corresponds to the centroid of the Fornax stellar density peak in the 500 pixel circle; units on the axes are arcminutes. We can see that, within the survey area, at least, the distribution of RR Lyraes (*upper left*) is apparently uniform, except for a small patch of variables that is associated with the outskirts of the rich globular cluster 3 lying just beyond the northern end of this region:[5] within the field covered here, there is no evident central concentration or radial falloff of the field RR Lyraes in Fornax. We are forced to conclude that the apparent offset of the RR Lyrae population to the north and west of the main body of Fornax results simply from the fact that more than half of the survey area lies to the north and west of Fornax’s density peak. Thus, we have no real constraint on the relative offset of the centroids of the old and intermediate-age populations in Fornax. Similarly, the rms radius of the RR Lyrae distribution is essentially that imposed solely by the boundaries of the survey area. The intermediate-age clump stars (*top right*), on the other hand, do begin to show a marginal falloff in density toward the edges of the survey area, especially to the north and west where the survey field extends farthest from the center of Fornax. Therefore, at least we can say that the intermediate-age population is more centrally concentrated than the oldest population but cannot at present say by how much. It is this greater central concentration that causes the distribution of intermediate-age stars to be less severely censored by the survey boundary, producing the apparent net offset between them and the RR Lyraes. Within the limitations of the present sample,

[5] Note that there is no evidence of a concentration of RR Lyraes near the position of the less populous globular cluster 4, which lies within the survey area. These observations are consistent with the estimated metallicities of these clusters: [Fe/H] = −2.1 for cluster 3 and −1.4 for cluster 4 (Buonanno et al. 1985; Dubath, Meylan, & Mayor 1992).

TABLE 2
MEAN LOCATIONS OF STELLAR POPULATION PROXIES IN AT LEAST EIGHT FRAME PAIRS

Sample	$+\Delta x$ = North (arcsec)	$+\Delta y$ = West (arcsec)	rms Radius (arcsec)	N
RR Lyraes	+46	+228	657	600
Clump	−42	+203	594	7969
Blue	−13	+212	521	1457
Red (a)	−66	+153	509	41
Red (b)	−44	+190	600	85
All	−45	+198	582	58310

no deviation from azimuthal symmetry is obvious in the distribution of red clump stars. It is possible that there is a local maximum in their density near (0, 0) in this figure, and it may also be that the outer isopleths appear to be centered somewhat to the south and west of (0, 0), but it is hard to be sure.

The blue main-sequence stars in Fornax (*bottom left*), conversely, display a clearly flattened distribution on the sky, with a long axis in the east-west direction and an axial ratio of order 3 or 4 to 1. The 26 most luminous blue stars—those with "V" < 20.00, represented by larger filled symbols in the figure—appear to be concentrated toward the opposite ends of the "bar" of blue main-sequence stars. (The puff of blue stars at the center of the northern edge of the field is presumably RR Lyraes or blue horizontal-branch stars associated with globular cluster 3.) Like the RR Lyraes, the blue stars in Fornax are offset to the north and west of the principal peak of stellar density; unlike the RR Lyraes, the blue stars are *more* centrally concentrated than the red clump stars, so the perceived offset *cannot* be imposed entirely by the geometry of the survey area. It must instead be real (at a 2.0 σ significance level if we compare the blue stars to the clump stars, 2.5 σ if we compare the blue stars to "all" Fornax stars). With a sample of only 126, it is difficult to say much about the distribution of the luminous red stars (*bottom right*), except that—if anything—the distribution of "carbon" stars (class [a], *filled symbols*) may be flattened in a direction *orthogonal* to the flattening of the distribution of blue stars.

The scope of this discussion can be expanded outward in the radial direction simply by considering the total area of Fornax that is contained within at least one, rather than at least eight, frame pairs. The cost of doing this is that now we can no longer rely on the variability index as a tool for extracting a nearly pure sample of RR Lyrae variables as a proxy for the oldest, most metal-poor population. Accordingly, we consider all stars that appeared in at least one frame pair, drop the L limit on the RR Lyrae sample, and—to reduce the contamination of the old sample by the young, blue stars—redefine the blue edge of the RR Lyrae zone to be at $B - R = 0.25$, rather than 0.00 as before. All other magnitude and color limits are left unchanged. The results of this new analysis are given in Table 3 and illustrated in Figure 12. Here we finally do see some decline in the surface density of "RR Lyraes" toward the outer edge of the survey area, but it is also clear that we have introduced some centrally concentrated contamination in the form of some other type of object leaking into the sample. Table 3 suggests that this contamination now *dominates* the "RR Lyrae" sample, because by merely doubling the survey area and *reducing* the color range considered while releasing the variability criterion, we have increased the number of "RR Lyrae" candidates by a factor of 9. The spatial distribution of the newly defined "RR Lyrae" sample suggests that the contamination has an origin among the intermediate-age stars: apparently the intermediate-age component so completely overwhelms the old population that, even though only a tiny percentage of its stars falls within the "RR Lyrae" box in the CMD through photometric error or because they are in a rare evolutionary state, they still outnumber the true old, metal-poor horizontal-branch stars. Hence, we make no attempt to derive a quantitative estimate of the effective radius of the RR Lyrae population in Fornax.

With the enlargement of the sample area we can reconsider the spatial distribution of the clump stars, by repeating our earlier centroiding exercise with the 2000, 1500, 1000, and 500 pixel circles, only this time we will consider *only* those stars with 21.00< "V" < 21.60 and $1.05 < B - R < 1.25$. Doing this, we find that—counting from the 2000 pixel circle to the 500 pixel one—the median centroids are at pixel positions (747, 916), (824, 828), (888, 651), and (983, 496) based on 8322, 5655, 2944, and 842 stars, respectively. The equinox 2000.0 equatorial coordinates of the first and last of these points are $02^h39^m52^s.7$, $-34°31'05''$ and $02^h40^m07^s.5$, $-34°29'21''$, respectively, and the position angle of the great circle connecting these two points is 63°. The centroids of the four circles are shown in the bottom right panel of Figure 11, with plusses for all of Fornax, and crosses for the clump stars. (Although these are based on counts of the full survey area, we display them on the map of the area contained in eight frame pairs for the more advantageous scale and crowding conditions.) As may be seen, both sequences show a nice linear progression toward the northeast as the stellar density peak is more and more narrowly defined. The 500 pixel centroid of the red clump stars is nearly coincident with the 500 pixel centroid of Fornax as a whole: they are separated by only 12″, which is less than the measuring error of the former. On the other hand, the 2000

TABLE 3
MEAN LOCATIONS OF STELLAR POPULATION PROXIES IN AT LEAST ONE FRAME PAIR

Sample	$+\Delta x$ = North (arcsec)	$+\Delta y$ = West (arcsec)	rms Radius (arcsec)	N
"RR Lyraes"	−37	+195	741	5395
Clump	−61	+202	756	11396
Blue	−27	+179	592	1670
Red (class [a])	−53	+64	595	47
Red (class [b])	−48	+173	736	114
All	−59	+194	735	80468

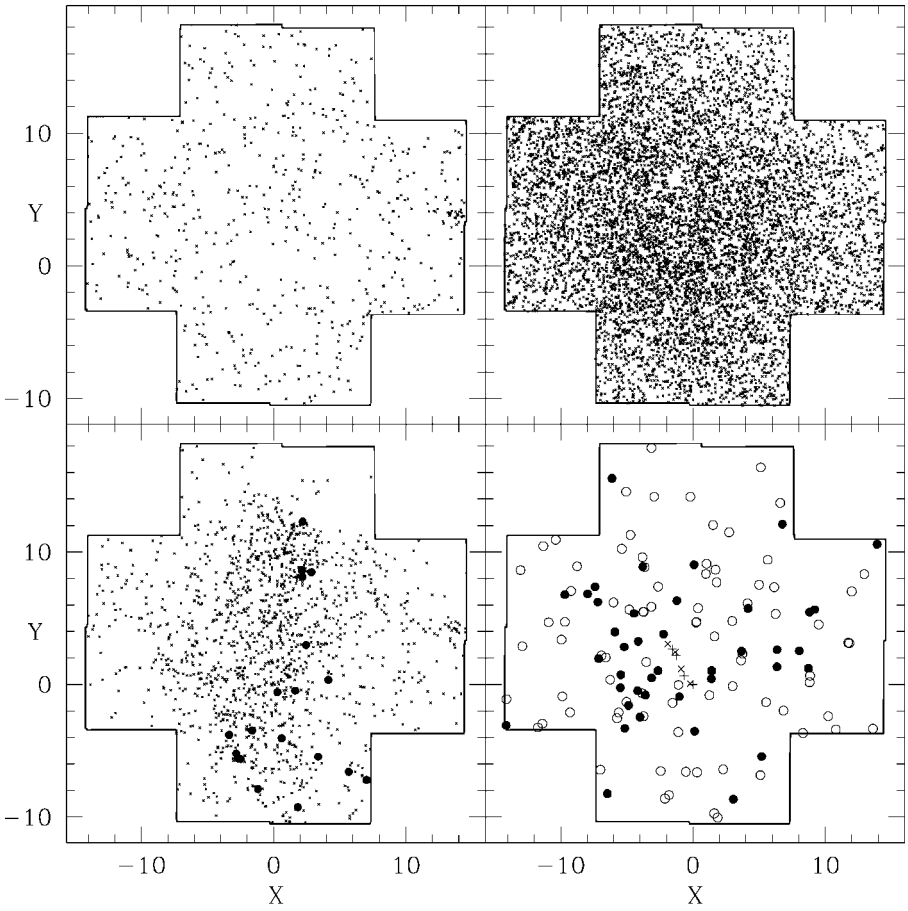

FIG. 11.—Distribution in the plane of the sky of several stellar-population proxies in the Fornax field: (*top left*) probable and highly probable RR Lyrae stars; (*top right*) stars in the region of the red horizontal-branch clump, presumably dominated by intermediate-age stars; (*bottom left*) bright blue stars apparently defining a very young main sequence (larger filled symbols are for the most luminous stars, with "*V*" < 20.00, smaller symbols are for the rest); and (*bottom right*) two varieties of luminous red stars, probable carbon stars with $B - R > 3.2$ (*filled circles*), and possible M stars with $2.7 < B - R \leq 3.2$ (*open circles*). Solid lines delimit the survey area contained within a minimum of eight frame pairs. A sequence of pluses marks the run of Fornax centroids as defined in 2000, 1500, 1000, and 500 pixel circles, based on the full survey area. A sequence of crosses shows the same for just the red clump stars believed to represent the intermediate-age populations of Fornax. Axis units are arcminutes.

pixel centroid of the clump stars is southwest, by some 30″, of the 2000 pixel centroid of Fornax. If this difference is real, it suggests that the major-axis asymmetry of the star counts may be more extreme among the red clump stars—by implication, among the intermediate-age stars—than it is among the totality of the populations in Fornax.

In the larger survey area the blue stars retain their more concentrated, flattened distribution. Indeed, given the likelihood that at least some of these blue stars may be RR Lyraes or blue horizontal-branch stars of Fornax's oldest stellar population, the true distribution of the young, blue stars is likely to be even more concentrated and flattened than it appears here. The spatial distribution of the slightly enlarged sample of class (a) extremely red giants continues to resemble that of the blue main-sequence stars and the class (b) very red giants are still like the red clump stars, according to Table 3, but the number statistics have not improved in a major way.

3.6. Cluster 6

In his early discussion of the globular clusters in Fornax, Shapley (1939) identified a faint object lying some 7′ north of globular cluster 4 as a possible additional cluster belonging to the galaxy. Hodge (1961a) described it as a group of five stars of approximately 21st magnitude; the implication was that he regarded its reality as a cluster to be dubious. As recently as 1994, Demers et al. considered the existence of the cluster as still worthy of debate, but stated that in their opinion the region contained "too few stars to be called a cluster."

The asterism known as cluster 6 was contained within nine

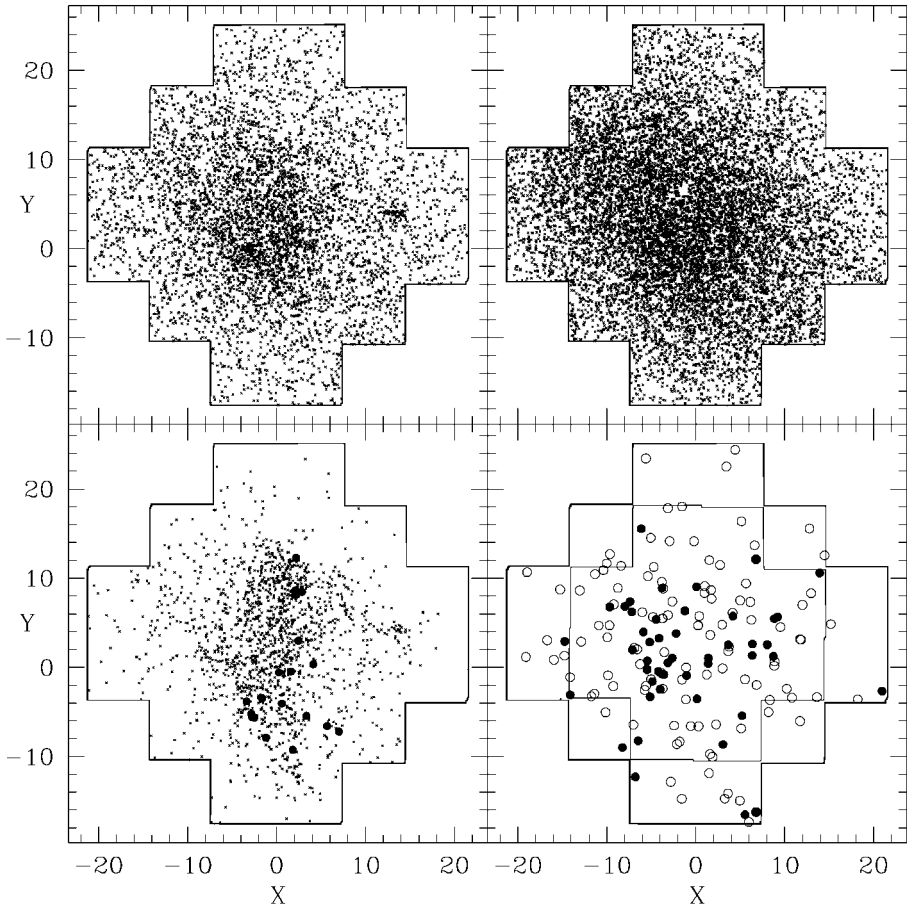

FIG. 12.—Same as Fig. 11, except that this is for the entire survey area contained within at least one frame pair—as delimited by the solid lines in the four panels—and the working definition of "RR Lyrae candidate" has been changed as outlined in the text. In the bottom right panel, the subarea contained within a minimum of eight frame pairs is also shown, for comparison.

of our frame pairs, and the depth and dynamic range of our stacked image allows us to contribute a new (as far as we can tell) observation to the discussion: nearly half of the "stars" in cluster 6 appear to us to be nonstellar and seem to constitute a very faint compact group of galaxies. In particular, utilizing the numbering scheme of Verner et al. (1981), objects 13, 19, 25, 39, 40, and 41 appear to be distinctly nonstellar in form. Several of the other, unnumbered objects in the area also appear to be nonstellar, such as an object 2″ to the east of "star" 39, another 3″ to the northeast of 39 (the western object of a 1″ pair), an object 4″ to the west of star 44, and a pair of objects 2″ north-northeast of 13. The degree of resolution of these objects is very slight, and it takes some playing with the brightness and contrast controls of the image display to convince oneself that their surface brightness is somewhat too low for their integrated fluxes, in comparison to nearby stars of similar apparent magnitude. There appear to be some other faint objects that cluster in this region, but they are so near the detection limit that we cannot judge which might be stars and which galaxies. We therefore conclude that at least part of "cluster 6" might still be worthy of further investigation, but as a very distant compact group of galaxies rather than as a star cluster.

4. SUMMARY

We have presented calibrated, precise photometry in the B and R filters for $\sim 10^5$ stars in a field of approximately $\frac{1}{3}$ deg^2 near the middle of the Fornax dwarf spheroidal galaxy. We catalog a number of very red stars in Fornax, including several not previously identified. In the CMD, the spectroscopically confirmed carbon stars form a long red tail with $B-R$ colors mostly greater than 3.2 mag. A clump of luminous red stars semidetached from the tip of the red giant branch appears to contain mostly oxygen-rich M stars, based on the subsample with published spectral classes. We are able to distinguish several populations of variable stars, including highly probable RR

Lyrae stars, probable anomalous Cepheids, and possible foreground eclipsing binaries. In addition, we identify a population of blue stars that appears to represent the tip of a very young ($\sim 10^8$ yr) main-sequence population.

After analyzing the spatial distribution of all stars in Fornax in general and each of these subpopulations in particular, we conclude that Fornax as a whole is divided into three parts: (*a*) the oldest population, represented by the RR Lyrae variables, is the most widely dispersed on the sky; (*b*) the intermediate-age population that produces the red core-helium-burning clump stars is the dominant component of the galaxy, is somewhat more centrally concentrated than the oldest population, and does not display elliptical symmetry on the sky, but rather the stellar density peaks several arcminutes to the northeast of the centroid of the outermost isopleths (on the other hand, the intermediate-age population in Fornax may display bilateral symmetry about an axis lying in a northeast-southwest direction); and (*c*) there is a small, young population revealed by the presence of luminous blue main-sequence stars that is more centrally concentrated than either the old or intermediate-age populations; it has a flattened distribution on the sky and its major axis is offset by roughly 30° from the symmetry axis of the galaxy as a whole. The very reddest and most luminous giant stars—most of which are carbon stars—appear to be as centrally concentrated as the youngest stars, while a distinct set of not quite so red luminous stars—some of which have been determined to be of spectral class M—are distributed rather more like the intermediate-age stars; however, this result is weak because of small-number statistics.

Present data cannot show definitively whether the young blue stars occupy a prolate spheroid, an edge-on oblate spheroid, or a disk tilted to the line of sight. However, there is a hint that the very youngest of these stars may be concentrated toward the two ends of the perceived distribution, suggesting a bilateral rather than a rotationally symmetric structure. The assertion that the reddest carbon stars are associated with the youngest population and that the not-so-red luminous giants are associated with the intermediate-age population is extremely vulnerable to small-number statistics, and it is not likely that it will be possible to materially enlarge the sample in the future. It will therefore be necessary to obtain kinematic or some other type of independent information to resolve this question.

We are grateful to Manuel Hernández and the Cerro Tololo staff for their usual exemplary assistance.

REFERENCES

Aaronson, M., & Mould, J. 1980, ApJ, 240, 804
Azzopardi, M., & Lequeux, J. 1992, in IAU Symp. 149, The Stellar Populations of Galaxies, ed. B. Barbuy & A. Renzini (Dordrecht: Kluwer), 201
Baade, W. 1944, ApJ, 100, 137
Beauchamp, D., Hardy, E., Suntzeff, N. B., & Zinn, R. 1995, AJ, 109, 1628
Bertelli, G., Bressan, A., Chiosi, C., Fagotto, F., & Nasi, E. 1994, A&AS, 106, 275
Buonanno, R., Corsi, C. E., Fusi Pecci, F., Hardy, E., & Zinn, R. 1985, A&A, 152, 65
Carney, B. W., & Seitzer, P. 1986, AJ, 92, 23
Da Costa, G. S. 1984, ApJ, 285, 483
———. 1997a, in ASP Conf. Ser. 116, The Second Stromlo Symposium: The Nature of Elliptical Galaxies, ed. M. Arnaboldi, G. S. Da Costa, & P. Saha (San Francisco: ASP), 270
———. 1997b, in Proc. VIII Canary Islands Winter School, Stellar Astrophysics for the Local Group: A First Step to the Universe, ed. A. Aparicio & A. Herrero (Cambridge: Cambridge Univ. Press), in press
Dearborn, D. S. P., Liebert, J., Aaronson, M., Dahn, C. C., Harrington, R., Mould, J., & Greenstein, G. L. 1986, ApJ, 300, 314
Demers, S., & Irwin, M. J. 1987, MNRAS, 226, 943
Demers, S., Irwin, M. J., & Kunkel, W. E. 1994, AJ, 108, 1648
Demers, S., & Kunkel, W. E. 1979, PASP, 91, 761 (DK)
Dubath, P., Meylan, G., & Mayor, M. 1992, ApJ, 400, 510
Fahlman, G. G., Mandushev, G., Richer, H. B., Thompson, I. B., & Sivaramakrishnan, A. 1996, ApJ, 459, L65
Frogel, J. A., Blanco, V. M., McCarthy, M. F., & Cohen, J. G. 1982, ApJ, 252, 133
Graham, J. A. 1982, PASP, 94 244
Green, P. J., Margon, B., & MacConnell, D. J. 1991, ApJ, 380, L31
Grillmair, C. J., et al. 1997, preprint (astro-ph/9709259)
Hodge, P. W. 1961a, AJ, 66, 83
Hodge, P. W. 1961b, AJ, 66, 249
Hodge, P. W., & Smith, D. W. 1974, ApJ, 188, 19
Kinman, T. D., Kraft, R. P., & Suntzeff, N. B. 1981, in Proc. Second Workshop on the Physical Processes in Red Giants, Physical Processes in Red Giants, ed. I. Iben, Jr., & A. Renzini (Dordrecht: Reidel), 71
Kormendy, J. 1985, ApJ, 295, 73
Landolt, A. U. 1973, AJ, 78, 959
———. 1992, AJ, 104, 340
Lee, M. G., Freedman, W., Mateo, M., Thompson, I., Roth, M., & Ruiz, M.-T. 1993, AJ, 106, 1420
Lehnert, M. A., Bell, R. A., Hesser, J. E., & Oke, J. B. 1992, ApJ, 395, 466
Light, R. M., Armandroff, T. E., & Zinn, R. 1986, AJ, 92, 43
Lundgren, K. 1990, A&A, 233, 21
Mateo, M., et al. 1994, BAAS, 185, 5103
Mateo, M., Udalski, A., Szymanski, M., Kaluzny, J., Kubiak, M., & Krzeminski, W. 1995, AJ, 109, 588
Mighell, K. J. 1990, A&AS, 82, 1
Mighell, K. J., & Butcher, H. R. 1992, A&A, 255, 26
Mighell, K., & Rich, R. M. 1996, AJ, 111, 777
Olszewski, E. W., & Aaronson, M. 1985, AJ, 90, 2221
Sarajedini, A., & Layden, A. C. 1995, AJ, 109, 1086
Shapley, H. 1938, Harvard Bull., 308
———. 1939, Proc. Natl. Acad. Sci. US, 25, 565
Smecker-Hane, T. A. 1997, in AIP Conf. Proc. 393, Seventh Astrophysics Conf., Star Formation Near and Far, ed. S. Holt & L. G. Mundy (New York: AIP), 571
Smecker-Hane, T. A., Stetson, P. B., Hesser, J. E., & Lehnert, M. D. 1994, AJ, 108, 507
Smecker-Hane, T. A., Stetson, P. B., Hesser, J. E., & VandenBerg, D. A. 1996, in ASP Conf. Ser. 98, From Stars to Galaxies: The Impact of Stellar Physics on Galaxy Evolution, ed. C. Leitherer, U. Fritze–van Alvensleven, & J. Huchra (San Francisco: ASP), 328

Smecker−Hane, T. A., et al. 1998, in preparation
Smith, H. A. 1995, RR Lyrae Stars (Cambridge: Cambridge Univ. Press)
Stetson, P. B. 1984, PASP, 96, 128
———. 1987, PASP, 99, 191
———. 1993, in IAU Colloq. 136, Stellar Photometry, Current Techniques and Future Developments, ed. C. J. Butler & I. Elliot (Cambridge: Cambridge Univ. Press), 291
———. 1994, PASP, 106, 250
———. 1996, PASP, 108, 851
———. 1997, Baltic Astron., 6, 3
———. 1998, in preparation
Stetson, P. B., McClure, R. D., & VandenBerg, D. A. 1985, PASP, 97, 908
Suntzeff, N. B., Mateo, M., Terndrup, D. M., Olszewski, E. W., Geisler, D., & Weller, W. 1993, ApJ, 418, 208
Suntzeff, N. B., Olszewski, E. O., Kraft, R. P., Friel, E., Aaronson, M., & Cook, K. 1984, PASP, 96, 795
Verner, G., Demers, S., Hardy, E., & Kunkel, W. E. 1981, AJ, 86, 357
Welch, D. L., & Stetson , P. B. 1993, AJ, 105, 1813
Westerlund, B. E., Edvardsson, B., & Lundgren, K. 1987, A&A, 178, 41 (WEL)
Westerlund, B. E., Lequeux, J., Azzopardi, M., & Rebeirot, E. 1991, A&A, 244, 367
Zinn, R. 1978, ApJ, 225, 790
———. 1981, ApJ, 251, 52